Special Section: Model-Data Fusion in the Vadose Zone

Khan Zaib Jadoon*
Lutz Weihermüller
Benedikt Scharnagl
Michael B. Kowalsky
Michel Bechtold
Susan S. Hubbard
Harry Vereecken
Sébastien Lambot

We use full-waveform, integrated hydrogeophysical inversion of time-lapse, off-ground GPR data to estimate the soil hydraulic properties at a fixed location over a bare agricultural field. The results suggest that the proposed method is promising for mapping the shallow soil hydraulic properties at the field scale with a high spatial resolution.

K.Z. Jadoon, L. Weihermüller, B. Scharnagl, M. Bechtold, H. Vereecken, and S. Lambot, Agrosphere (IBG-3), Institute of Bio- and Geosciences, Forschungszentrum Jülich, GmbH, 52425 Jülich, Germany; K.Z. Jadoon, Water Desalination and Reuse Center, King Abdullah University of Science and Technology (KAUST), 23955-6900 Thuwal, Saudi Arabia; B. Scharnagl, now at Inst. Geoecology, Technische Universität Braunschweig, 38106 Braunschweig, Germany; M.B. Kowalsky and S. Hubbard, Earth Sciences Division, Lawrence Berkeley National Lab., Berkeley, CA 94720; M. Bechtold, now at Inst. of Agricultural Climate Research, Johann Heinrich von Thünen-Institut (vTI), 38116 Braunschweig, Germany; S. Lambot, Earth and Life Institute, Université catholique de Louvain, Croix du Sud, 2 box L7.05.02, Louvain-la-Neuve B-1348, Belgium. *Corresponding author (k.z.jadoon@fz-juelich.de).

Vadose Zone J.
doi:10.2136/vzj2011.0177
Received 23 Nov. 2012.

© Soil Science Society of America
5585 Guilford Rd., Madison, WI 53711 USA.
All rights reserved. No part of this periodical may be reproduced or transmitted in any form or by any means, electronic or mechanical, including photocopying, recording, or any information storage and retrieval system, without permission in writing from the publisher.

Estimation of Soil Hydraulic Parameters in the Field by Integrated Hydrogeophysical Inversion of Time-Lapse Ground-Penetrating Radar Data

An integrated hydrogeophysical inversion approach was used to remotely infer the unsaturated soil hydraulic parameters from time-lapse ground-penetrating radar (GPR) data collected at a fixed location over a bare agricultural field. The GPR model combines a full-waveform solution of Maxwell's equations for three-dimensional wave propagation in planar layered media together with global reflection and transmission functions to account for the antenna and its interactions with the medium. The hydrological simulator HYDRUS-1D was used with a two layer single- and dual-porosity model. The radar model was coupled to the hydrodynamic model, such that the soil electrical properties (permittivity and conductivity) that serve as input to the GPR model become a function of the hydrodynamic model output (water content), thereby permitting estimation of the soil hydraulic parameters from the GPR data in an inversion loop. To monitor the soil water content dynamics, time-lapse GPR and time domain reflectometry (TDR) measurements were performed, whereby only GPR data was used in the inversion. Significant effects of water dynamics were observed in the time-lapse GPR data and in particular precipitation and evaporation events were clearly visible. The dual porosity model provided better results compared to the single porosity model for describing the soil water dynamics, which is supported by field observations of macropores. Furthermore, the GPR-derived water content profiles reconstructed from the integrated hydrogeophysical inversion were in good agreement with TDR observations. These results suggest that the proposed method is promising for non-invasive characterization of the shallow subsurface hydraulic properties and monitoring water dynamics at the field scale.

Abbreviations: DP, dual porosity; GPR, ground-penetrating radar; MVG, Mualem–van Genuchten model; PEC; perfect electrical conductor; RMSE, root mean square error; TDR, time domain reflectometry.

Sustainable and optimal management of soil and water resources requires mathematical models that predict subsurface flow and transport processes. These models depend on the physical system geometry, boundary conditions and soil hydraulic properties such as the hydraulic conductivity and water retention functions (Gerke and van Genuchten, 1993). A full understanding of soil processes requires knowledge of the soil hydraulic properties and their spatial and temporal distributions. Many mathematical models exist for approximating subsurface flow processes in single- and dual-porosity systems (e.g., Mualem, 1976; van Genuchten, 1980; Durner, 1994; Assouline et al., 1998; Iden and Durner, 2007). A major shortcoming in the application of these models is the lack of knowledge regarding the spatial and temporal distributions of the model parameters at scales that are pertinent to management scales. In that respect, hydrogeophysical measurement methods have gained increasing attention for high-resolution characterization of the shallow subsurface at the field scale (Vereecken et al., 2008).

Surface-based ground-penetrating radar (GPR) has received considerable attention to estimate soil water content at shallow depth. GPR is particularly well adapted to noninvasively determine soil water content (Huisman et al., 2003). As the dielectric properties of water overwhelm those of other soil components, water and its spatial distribution strongly control GPR wave propagation in the soil. For instance, Grote et al. (2003) used the direct ground wave method to map the spatial distribution of soil water content across a vineyard. Several authors have used two way travel times from a reflector at known depth to monitor temporal changes of water content (Stoffregen et al., 2002; Lunt et al., 2005). A densely sampled reflection GPR survey can be conducted to monitor the

soil water dynamics in unsaturated sandy alluvial sediments after forced infiltration (Haarder et al., 2011). Moysey (2010) studied the sensitivity of hydrologic processes linked to the wetting and drying events observed in the GPR arrival, e.g., the ground wave and reflection. Despite the success of surface-based GPR for estimating soil water content, there are several challenges in using it to constrain dynamic hydrological processes in soil. For instance, Jacob and Hermance (2004) reported the limited precision with which GPR travel times and velocities can be determined from data in practice.

Tomographic inversion of GPR data has been used in different studies to estimate the hydrogeological parameters (Holliger et al., 2001; Binley et al., 2002b). These conventional GPR inversion schemes suffer from two major shortcomings. First, in most cases the forward model describing the electromagnetic wave propagation is assumed to be one-dimensional (plane wave) and the straight-ray approximation is used, which results in inherent errors in the reconstructed water content images. Moreover, this does not permit the exploitation of all the information contained in the radar data. One way to overcome such shortcomings is by performing full-waveform forward and inverse modeling of the GPR data, which has become feasible with advances in computing resources (Lambot et al., 2004c; Gloaguen et al., 2007a; Klotzsche et al., 2010; Lambot et al., 2012). A second problem arises from non-uniqueness and other optimization issues that arise in reconstructing subsurface images. The inverse problem is usually constrained by providing additional information through smoothness conditions or more advanced geostatistical models (Giroux et al., 2007; Gloaguen et al., 2007b), or by including data from additional sensors (Ghose and Slob, 2006; Linde et al., 2006; Kowalsky et al., 2008). A promising approach for time-lapse analysis is to resort to integrated, often referred to as joint, hydrogeophysical inversion techniques, where the geophysical and hydrodynamic models constrain each other (Rucker and Ferré, 2004; Kowalsky et al., 2005; Lambot et al., 2010). In that way, the possible water content distributions are not only limited to those respecting the physical laws of electromagnetics but also the laws of hydrodynamics, thereby reducing significantly the solution space and complexity of the optimization problem. Hinnell et al. (2010) compared the abilities of coupled and uncoupled hydrogeophysical inversion using a synthetic example of one-dimensional infiltration and showed that the coupled approach can provide significant reductions in uncertainty for hydrologic properties and associated predictions.

In the last few decades, time-lapse GPR measurements have shown great potential for field-scale characterization and imaging of soil hydrogeophysical properties (Hubbard and Rubin, 2000; Slob et al., 2010). In particular, time-lapse GPR imaging can be used to characterize natural drainage inside the vadose zone (Truss et al., 2007). Time-lapse GPR measurements further permit the monitoring of subsurface flow processes and inference of the soil hydraulic properties when coupled with soil hydrodynamic modeling. This has been applied to cross-hole GPR, where one- or two-dimensional time-lapse images of the soil water content are obtained from travel-time tomography analysis and subsequently inverted to retrieve key soil hydraulic parameters (Binley et al., 2002a; Rucker and Ferré, 2004; Cassiani and Binley, 2005; Looms et al., 2008). In all such studies, the soil medium is considered as a single porosity system and the water retention and hydraulic conductivity functions, respectively, are based on the Mualem and van Genuchten model (Mualem, 1976; van Genuchten, 1980). It is well known that structural properties such as aggregation and macro-porosity influence the soil hydraulic behavior (Weynants et al., 2009). In the majority of silt-loam soils, macro-pores are present and the dual-porosity model can best explain the water retention and hydraulic conductivity functions (Weynants, 2011).

Cross-borehole GPR techniques are useful for characterization scales of a few meters, whereas surface or proximal GPR is needed to cover large areas such as agricultural fields. For this application, Lambot et al. (2004c) proposed a full-waveform forward and inverse modeling approach, which is well suited for off-ground GPR. The radar system is set up using vector network analyzer technology, thereby providing standard, frequency domain measurements of well-known physical quantities. The electromagnetic model is based on a specific solution of the three-dimensional Maxwell equations for waves propagating in multilayered media, describing locally the air and subsurface, and on linear transfer functions in series and in parallel to account for antenna effects and antenna-soil interactions. The electromagnetic model was shown to be very accurate in describing the radar measurements and model inversion was successfully applied to retrieve the properties of two soil layers under laboratory conditions (Lambot et al., 2004c) or to identify and map surface soil moisture in the field (Jonard et al., 2011; Minet et al., 2012). In all these studies, the inverse problem was well-posed given the relatively simple configurations dealt with and the corresponding limited number of unknowns. In particular, the proposed method was used to monitor water content dynamics in a laboratory soil column subject to a drainage event (Lambot et al., 2004a). The time-lapse soil moisture data obtained in that way were subsequently used in a hydrodynamic inversion scheme to identify the unsaturated soil hydraulic properties. In that experimental setup, monitoring was performed from the side of the soil column with a perfect electrical conductor (PEC) as the boundary condition, thereby reducing the electromagnetic model to a simple, vertically layered configuration (air-plastic-soil-PEC).

In field conditions, the number of layers is typically unknown and soil moisture profiles vary piecewise continuously with depth, resulting in an inherently ill-posed electromagnetic inverse problem with a large number of unknowns. In that case, resorting to a joint electromagnetic-hydrodynamic inversion scheme, as introduced by Lambot et al. (2006b), appears to be necessary. We

showed that with such integrated inversion, elemental uniqueness and stability conditions of the inverse problem are theoretically satisfied for a range of different soils and hydrodynamic boundary conditions (Jadoon et al., 2008). This means that enough information may be contained in the time-lapse, off-ground GPR data to estimate the soil hydraulic properties. Only in highly electrically conductive soils or in the absence of reflecting profiles are limitations expected due to the decreased information content of the radar data. Lambot et al. (2009) validated the proposed approach in a laboratory sand with different infiltration events. The time-lapse GPR data can be acquired in a soil mapping context, which potentially provides a means to map the soil hydraulic properties with high spatial resolution at the field scale.

In this paper, we extend the analysis of Jadoon et al. (2008) and Lambot et al. (2009) to field conditions, where the unsaturated soil hydraulic properties of a soil are remotely estimated from time-lapse GPR measurements. A low frequency horn antenna operating in the frequency range 0.2–2.0 GHz was used and the antenna was fixed at one location at a height of about 110 cm above the ground. Within the foot-print of the GPR antenna, the surface of the soil was exposed to natural conditions, such as evaporation and precipitation. Time-lapse TDR and GPR measurements were performed for twenty days and three major precipitation events occurred during that period. Soil hydraulic parameters were estimated for single-and dual-porosity models by integrated hydrogeophysical inversion. Results were compared to the water content profiles obtained by TDR and soil hydraulic properties were estimated from undisturbed soil samples.

Material and Methods

Integrated Hydrogeophysical Inversion

Inversion Flowchart

The joint electromagnetic and hydrodynamic inversion procedure applied in this study is depicted in Fig. 1. Inversion is formulated as a classical least-squares problem, where an objective function describing the discrepancies between the measured and modeled radar data is minimized iteratively by means of an optimization algorithm. In this study, only time-lapse geophysical data were included in the objective function though additional information such as hydrological data can also be included (Kowalsky et al., 2005). The presented method is applicable to ultra wideband stepped-frequency continuous-wave monostatic GPR, for which accurate full-waveform forward modeling can be performed (Lambot et al., 2004c). It is worth mentioning that in the inversion flowchart, antenna effects are first filtered out from the raw radar data using a radar-antenna model. The inverted radar data are thereby expressed in terms of a frequency dependent, time-lapse Green's function [$G_{xx}^{\uparrow}(f,t)$], which represents the backscattered electric field normalized to a unit-strength electric source. The Green's function is therefore independent of the source.

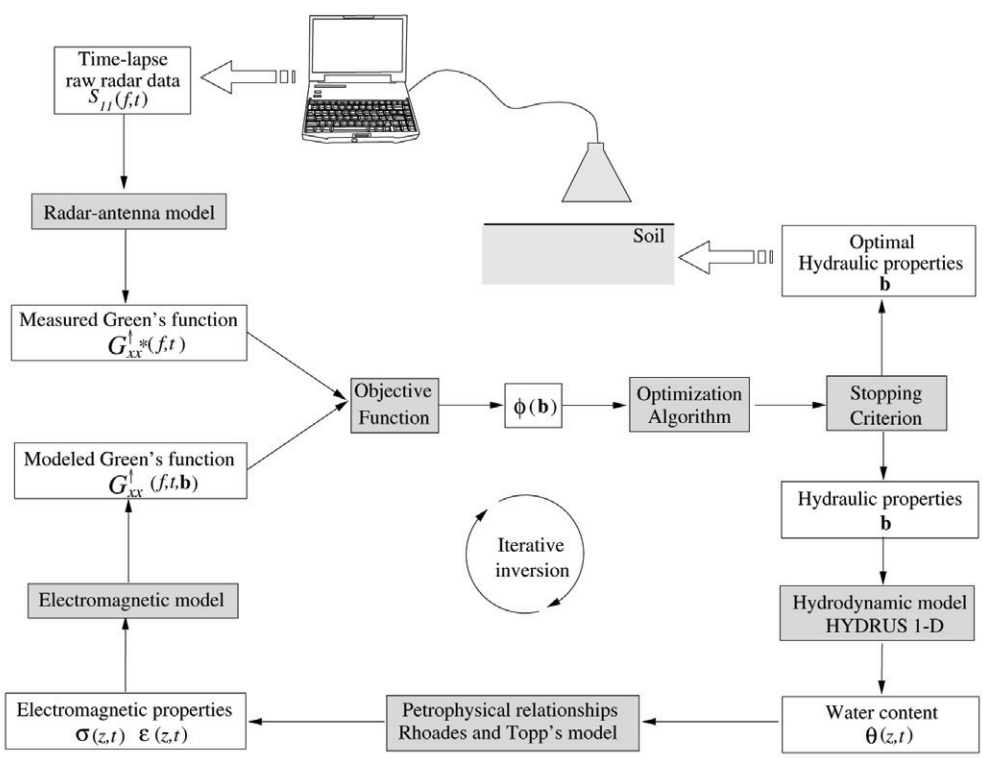

Fig. 1. Flowchart representing the integrated electromagnetic and hydrodynamic inversion of time-lapse radar measurements for estimating soil hydraulic properties and electric profiles (t is time, z is depth, and f is frequency) (Lambot et al., 2006b). Shaded boxes denote operators and white boxes denote variables.

With this inversion scheme, the traditional electromagnetic inverse problem for reconstructing electromagnetic and correlated water content profiles is constrained by a hydrodynamic model. In that case, the solution space significantly reduces, as possible electromagnetic profiles cannot be arbitrary but should respect soil hydrodynamic laws. The parameters to be estimated reduce to the soil hydraulic properties. Time-lapse radar data are therefore necessary as well as information regarding the hydrodynamic status, such as initial conditions as well as boundary conditions. In addition, the soil-specific relationships relating the hydrological variables of interest to the soil electromagnetic properties should be known. Although the relationship between soil dielectric permittivity and water content is comparable for various soil types (Topp et al., 1980), the relation between electrical conductivity, water content, and salinity may be subject to larger uncertainties (Rhoades et al., 1990).

Electromagnetic Model

The measured and modeled time-lapse GPR data are represented by the full-waveform, frequency domain GPR Green's functions $G_{xx}^{\uparrow *}(f,t)$ and $G_{xx}^{\uparrow}(f,t,\mathbf{b})$, respectively, defined for wave propagation in three-dimensional multilayered media, where f is frequency, t is time for the time-lapse GPR measurement, and $\mathbf{b}$ is the unknown parameter vector for the soil hydraulic properties. Hence, the electromagnetic model assumes the soil to be locally homogeneous in the horizontal directions, i.e., at the GPR measurement scale (about 1 m^2). The Green's function is defined as the backscattered (upward component denoted by the up arrow in $G_{xx}^{\uparrow}$), x-directed electric field (first subscript x in $G_{xx}^{\uparrow}$) at the antenna phase center for a unit-strength, x-directed electric source (second subscript x in $G_{xx}^{\uparrow}$) situated at the same position above the multilayered medium. The antenna phase center represents the origin of the radiated field from which the far-field spherical divergence is initiated.

Solutions of Maxwell's equations for wave propagation in three-dimensional multilayered media are well known (Michalski and Mosig, 1997). We derived this specific Green's function using a recursive scheme to compute the transverse electric and magnetic global reflection coefficients of the multilayered medium in the spectral domain (Slob and Fokkema, 2002; Lambot et al., 2004c). The transformation back to the spatial domain is performed by evaluating numerically a semi-infinite, complex integral. A specific procedure was applied for a fast and accurate evaluation of that integral (Lambot et al., 2007), which inherently contains singularities.

The constitutive parameters governing electromagnetic wave propagation in the soil are the dielectric permittivity ε (Fm^{-1}), electrical conductivity σ ($S\ m^{-1}$), and magnetic permeability μ (Hm^{-1}). These properties characterize each layer of the multilayered model. In this paper, we assume μ to be equal to the permeability of free space, namely, $\mu_0 = 4\pi \times 10^{-7}\ Hm^{-1}$, which is valid for non-magnetic soil materials as is prevalent in the environment. The relative dielectric permittivity is defined as $\varepsilon_r = \varepsilon/\varepsilon_0$, where $\varepsilon_0 = 8.85 \times 10^{-12}\ Fm^{-1}$ is the dielectric permittivity of free space. A continuous variation of the electromagnetic properties with depth can be emulated using a fine discretization of the multilayered medium compared to the minimal wavelength. Typically, the layers should be thinner than one tenth of the minimal wavelength. Electromagnetic wave reflection on a bare soil is dependent on the surface roughness. A differentiation between smooth and rough surfaces can be made with respect to the wavelength of the signal based on the Rayleigh criterion ($h_c = \lambda/8$), where h_c is the critical height of the surface protuberances, and λ is the wavelength. If the surface is smooth and homogeneous (in terms of electrical properties), most of the energy reflected will be in the specular direction (coherent component), while if the surface is rough, diffuse reflections or scattering (incoherent component) can occur leading to less energy being recorded in the specular direction. Recently, Jonard et al. (2012) combined the roughness model with the full-waveform off-ground GPR model proposed by Lambot et al. (2004c) and the approach was tested in a controlled laboratory experiment. In this study, the surface roughness model is not included in the radar model, which can be justified when the surface of the soil is kept relatively smooth.

For a monostatic mode of operation, i.e., the same antenna simultaneously plays the role of transmitter and receiver, the sensitivity of the radar measurements with respect to the horizontal variations of the soil electromagnetic properties is expected to be limited. In addition, when the antenna is far enough from the soil surface, the spatial distribution of the backscattered electric field over the antenna aperture tends to be independent of the soil electromagnetic properties and their spatial distribution, i.e., only the phase and amplitude of the electric field change (plane wave approximation). As a result, and owing to the linearity of Maxwell's equations, the following equation can be used to model the antenna and its multiple interactions with the soil (Lambot et al., 2004b):

$$S_{11}(\omega) = \frac{b(\omega)}{a(\omega)} = H_i(\omega) + \frac{H(\omega)G_{xx}^{\uparrow}(\omega)}{1 - H_f(\omega)G_{xx}^{\uparrow}(\omega)} \qquad [1]$$

where $S_{11}(\omega)$ is the measured (raw radar data) frequency-dependent ratio between the backscattered $b(\omega)$ and incident $a(\omega)$ electric fields at the calibration plane of the vector network analyzer, $H_i(\omega)$, $H(\omega)$, and $H_f(\omega)$, are the characteristic antenna transfer functions accounting for antenna propagation effects and antenna-soil interactions, $G_{xx}^{\uparrow}$ is the transfer Green's function of the air-subsurface system modeled as a three-dimensional multilayered medium, and ω is the angular frequency ($\omega = 2\pi f$). The antenna transfer functions act as global transmittances and reflectances and account for all variations of impedance from the calibration plane of the vector network analyzer (antenna connector) to the air and vice-versa. The characteristic antenna transfer functions can be determined by solving a system of equations as Eq. [1] to these three unknown functions, by performing S_{11} measurements

for known configurations, i.e., for which the Green's functions $G_{xx}^{\uparrow}$ can be computed (Lambot et al., 2004c, 2006a). Generally, measurements are performed with the antenna located at different heights above a perfect electrical conductor (e.g., a copper sheet). Once the antenna transfer functions are known, antenna effects can be removed from the raw radar data and the Green's function, containing only the response of the air-soil, can be derived (using Eq. [1]). The antenna transfer functions used in the radar model inherently account for the frequency dependent phase center position of the antenna (Jadoon et al., 2011).

Hydrodynamic Model

In this study, we considered one-dimensional vertical water flow in a homogeneous and isotropic rigid porous medium, whose hydrodynamics is described by Richards' equation, expressed here in terms of pressure head:

$$C(h)\frac{\partial h}{\partial t}=\frac{\partial}{\partial z}\left[K(\theta)\left(\frac{\partial h}{\partial z}-1\right)\right] \quad [2]$$

where h is the time- and depth-dependent pressure head (cm), $C(h) = d\theta(h)/dh$ is the differential water capacity with $\theta(h)$ being the water content as a function of pressure head ($cm^3\ cm^{-3}$), θ being the volumetric water content ($cm^3\ cm^{-3}$), $K(\theta)$ is the hydraulic conductivity as a function of water content ($cm\ h^{-1}$), t is the time (hr), and z is the depth taken positive downward (cm).

The classical Mualem-van Genuchten (MVG) model (Mualem, 1976; van Genuchten, 1980) and the dual porosity (DP) model as proposed by Durner (1994) were used to describe the characteristic hydraulic properties (water retention and hydraulic conductivity functions) of the subsurface system. The water retention curve for a multi-model porous medium is given by:

$$\theta(h)=\theta_r+(\theta_s-\theta_r)\sum_{i=1}^{k}\omega_i S_i \quad [3]$$

$$S_i=\left[1+|\alpha_i h|^{n_i}\right]^{-m_i} \quad [4]$$

where θ_r and θ_s are the residual and saturated water contents ($cm^3\ cm^{-3}$), respectively, k is the order of the porosity in a system, ω_i are the weighting factors subject to $0 < \omega_i < 1$ and $\sum\omega_i=1$. The van Genuchten (1980) curve shape parameters α_i (cm^{-1}) and n_i (–) are inversely related to the air entry value and the width of the pore size distribution, respectively, and m_i is defined as $m_i = 1-1/n_i$ with $n_i > 1$. The hydraulic conductivity relationship is given by Priesack and Durner (2006):

$$K(\theta)=K_s\sum_{i=1}^{k}\omega_i S_i^{\lambda}\left[\frac{\sum_{i=1}^{k}\omega_i\alpha_i\left(1-\left(1-S_i^{1/m_i}\right)^{m_i}\right)}{\sum_{i=1}^{k}\omega_i\alpha_i}\right]^r \quad [5]$$

where K_s is the saturated hydraulic conductivity ($cm\ h^{-1}$), λ [–] is a factor that accounts for the pore tortuosity, and r determines the shape of the hydraulic conductivity function, with $r = 2$ according to Mualem (1976). In Eq. [3] and [5], the value of k = is 1 and 2, respectively, for the MVG and DP model.

The total number of hydraulic parameters in the MVG model is six, i.e., θ_r, θ_s, α, and n for the water retention curve, plus K_s and λ for the unsaturated hydraulic conductivity function. In the dual porosity model three additional parameters α^*, n^*, and ω^* are considered. Superscript * is used for additional parameters as compared to the MVG model. Parameter θ_r is usually defined as the residual water content corresponding to a value of $h \rightarrow -\infty$. Generally, this parameter is regarded as an empirical parameter and can be fixed either to a value which yields the best fit to the experimental water retention data (Kool et al., 1985), or to the value of zero (Nimmo, 1991; Fuentes et al., 1992). When considered different from zero, θ_r can be quite accurately inferred from soil texture using pedotransfer functions (Vereecken et al., 1989) or directly derived from radar measurements under extremely dry conditions at the soil surface (Lambot et al., 2006c). Similarly, θ_s can be directly obtained from radar measurements when the soil surface is saturated (Lambot et al., 2009; Jadoon et al., 2010). Parameter λ is generally considered to have a relatively small effect on the hydrodynamic events and can be either fixed to the generally used value of 0.5 or, preferably, estimated from bulk density and hydraulic conductivity with which it is highly correlated (Vereecken, 1995; Lambot et al., 2002). Mualem (1976) reported that λ equal to 0.5 was an optimal value for a data set of 45 disturbed and undisturbed samples. In many studies aiming to estimate the soil hydraulic properties from coupled hydrogeophysical inversion the parameter λ is fixed to 0.5 to minimize the number of unknowns, e.g., Looms et al. (2008); Hinnell et al. (2010); Huisman et al. (2010); Mboh et al. (2011, 2012a,b). Given these considerations, we assumed θ_r, θ_s, and λ to be known in the hydrogeophysical inversion process. This results in three parameters (α, n, K_s) to be estimated for the MVG model and six for the DP model (α, n, K_s, α^*, n^*, ω^*).

Equation [2] is solved numerically using the hydrological simulator HYDRUS-1D (Simunek et al., 2008). The depth of the simulation domain was fixed to z = 60 cm and the vertical profile was discretized into 120 equally sized elements, representing dz = 0.5 cm. From a profile description two horizons were distinguished, with a plow horizon A from 0 to 32 and a relatively homogenous deeper horizon B from 32–60-cm depth, which defined the simulation domain. In many agricultural fields, it might be reasonable to assume a conceptual two-layer system with the first layer being the plow horizon and assuming a spatially uniform thickness of this plow horizon. The time step for the top boundary condition (precipitation and evaporation) was fixed to 1 h and the time required to complete one hydrological computation is nearly 1.5 s on a normal PC. In this study the hydrological simulator HYDRUS-1D is used because of its simplicity, robust numerical

scheme, short calculation times and availability of soil hydraulic data for comparison. Harter and Hopmans (2004) reported that with respect to regional-scale flow processes, at sufficiently large scales and in the absence of interflow, the average lateral flow component is negligible, so that the large-scale Richard's equation becomes one-dimensional.

Petrophysical Relationships

Several empirical and conceptual relationships exist to relate soil dielectric permittivity to volumetric water content, which are highly correlated due to the overwhelming dielectric properties of water compared to other soil constituents. Empirical relationships are less complex than physical models as they require very limited information about soil textural properties, e.g., porosity, pore structure, bulk density (Steelman and Endres, 2011). For instance, Topp et al. (1980) proposed an empirical calibration between soil volumetric water content (θ) and apparent relative permittivity (ε_r):

$$\varepsilon_r = 3.03 + 9.3\theta + 14.6\theta^2 - 76.7\theta^3 \qquad [6]$$

In general, Topp's equation is widely used in coarse and medium-textured soils and has proved very successful. However, in some soils containing clays (Bridge et al., 1996) and organic matter (Schaap et al., 1997), or in aggregated (Miyamoto et al., 2003), or anisotropic porous media (Jones and Friedman, 2000), this equation does not describe the lower permittivity values often measured. Many other empirical equations have been presented that seek to incorporate the effects of soil texture and density to overcome this limitation (Ledieu et al., 1986; Roth et al., 1992; Malicki et al., 1996). Nevertheless, we used Topp's model, as for the same test site Topp's model was shown to provide good results (Weihermüller et al., 2007), with a root-mean-square error of 0.021 ($m^3\ m^{-3}$) between volumetric soil samples and TDR estimates.

The electrical conductivity of soil depends on the porosity, degree of saturation, clay content, and other bulk soil properties. In addition, conductivity of soil is affected by the frequency of the electromagnetic energy due to relaxation mechanisms that operate at different frequencies. In a soil mixture the relaxation mechanisms may be attributed to the solid material and the pore water as well as to interfacial phenomena. At frequencies below 1 GHz, soil electrical conductivity is weakly frequency-dependent and dielectric losses are generally low (Davis and Annan, 1989). Several frequency-independent models exist to relate soil electrical conductivity to volumetric water content. For instance, the equation proposed by Archie (1942) is one of the most widely used relationships for estimating the effective electrical conductivity responses of water-saturated lithology. The model of Rhoades et al. (1976) is commonly used to predict electrical conductivity of soils in terms of the water content. The Rhoades model considers the surface conductivity as a parameter that is independent of soil water content as follows:

$$\sigma = \left(c\theta^2 + d\theta\right)\sigma_w + \sigma_s \qquad [7]$$

where c and d are field specific fitting parameters (–), σ_w is the electrical conductivity of the water (Sm^{-1}), σ_s is the electric conductivity of the dry soil (Sm^{-1}), and θ is again volumetric water content ($cm^3\ cm^{-3}$). To reduce the number of parameters, Eq. [7] was simplified as:

$$\sigma = A\theta^2 + B\theta + \sigma_s \qquad [8]$$

where A is the product of c and σ_w, and B is the product of d and σ_w. Parameters A, B, and σ_s were inversely obtained by fitting the Rhoades model to a TDR dataset of simultaneous water content and bulk electrical conductivity measurements. Calibration of the petrophysical model at the field scale will not be straight forward. On a larger scale, maybe the field can be divided into zones with respect to the soil physical properties (texture, structure and bulk density) and petrophysical models can be calibrated for specific zones, or part of the petrophysical parameters can be considered as additional unknowns in the inversion process in the case they are not available.

Objective Function

The inverse problem for a complex quantity is formulated in the least-square sense in terms of electromagnetic data as follows:

$$\min \varphi(\mathbf{b}) = \sum_t \sum_f \left| G_{xx}^{\uparrow *}(f,t) - G_{xx}^{\uparrow}(f,t,\mathbf{b}) \right|^2 \qquad [9]$$

where $G_{xx}^{\uparrow *}(f,t)$ and $G_{xx}^{\uparrow}(f,t,\mathbf{b})$ are the vectors containing the observed and simulated Green's functions, respectively. Since the Green's functions are complex valued, the difference between observed and modeled data is expressed by the magnitude of the errors in the complex plane, thereby inherently accounting for both amplitude and phase information.

In this study, two inversion scenarios were performed for time-lapse radar data. In the first scenario, a single porosity model was used in full-waveform hydrogeophysical inversion to estimate six soil hydraulic parameters, $\mathbf{b} = [\alpha_1, n_1, K_{s1}, \alpha_2, n_2, K_{s2}]$, where subscripts 1 and 2 corresponds to two layers with different hydrological properties. In the second scenario, the A-horizon (top layer) was considered as a dual porosity system and three additional parameters (α_1^*, n_1^*, w_1) were optimized. In both inversions, the B-horizon (second layer) was considered as a single porosity system and the MVG model was used. The optimization parameters and are presented in Table 1. To properly deal with the nonlinearity of the objective function during minimization and, in particular, avoid being trapped in local minima, we adopted a global optimization approach. Hence, we used the shuffled complex evolution (SCE-UA) algorithm for the global optimization (Duan et al.,

Table 1. Inversely estimated soil hydraulic parameters obtained from mean of the retention datasets of ten undisturbed soil samples, and integrated hydrogeophysical inversion of time-lapse ground-penetrating radar (GPR) data by using Mualem–van Genuchten (MVG) and dual porosity (DP) model. MVG model has six parameters (θ_r, θ_s, α, n, K_s and λ) and three additional parameters (α^*, n^*, ω) are used for DP model. The parameter values marked with ‡ were fixed while remaining parameters were estimated by inversion.

		Undisturbed soil sample				GPR MVG inversion		GPR DP inversion	
	Parameter range	Layer 1	Layer 1	Layer 2	Layer 2	Layer 1	Layer 2	Layer 1	Layer 2
θ_r, cm^3 cm^{-3}	0.00–0.15	0.069	0.045	0.053	0.029	0.045‡	0.045‡	0.045‡	0.045‡
θ_s, cm^3 cm^{-3}	0.30–0.45	0.326	0.412	0.363	0.431	0.426‡	0.426‡	0.426‡	0.426‡
α, cm^{-1}	$(0.5–100)\times10^{-3}$	1.8×10^{-3}	1.4×10^{-3}	3.9×10^{-3}	1.6×10^{-3}	7.2×10^{-3}	2.1×10^{-3}	2.8×10^{-3}	2.7×10^{-3}
n	1.1–2.0	1.715	1.603	1.401	1.418	1.290	1.628	1.823	1.359
K_s, cm h^{-1}	0.05–80	20.610‡	20.610‡	23.870‡	23.870‡	13.550	4.015	11.794	4.363
λ	0.50	0.50‡	0.50‡	0.50‡	0.50‡	0.50‡	0.50‡	0.50‡	0.50‡
α^*, cm^{-1}	0.01–0.60	—	0.641	—	0.214	—	—	0.598	—
n^*	1.1–4.0	—	1.681	—	1.532	—	—	3.649	—
w	0.1–0.6	—	0.30	—	0.30	—	—	0.28	—

1992). This global optimization algorithm has been widely used in hydrologic modeling (Sorooshian et al., 1993) and proved to be consistent and efficient for finding the global optimum parameter values of hydrologic models (Vrugt et al., 2003).

The undisturbed soil sample parameters for the water retention function were estimated by inversion. The objective function was formulated in terms of least-squares as follows:

$$\varphi(\mathbf{b}) = \sum \left| \theta(h)^* - \theta(h, \mathbf{b}') \right|^2 \qquad [10]$$

where $\theta(h)^*$ and $\theta(h,\mathbf{b}')$ and are the vectors containing the observed and simulated water retention functions, respectively. For each A and B horizon, two inversions were performed by considering the undisturbed soil sample as a single- and dual-porosity system. Four parameters $\mathbf{b}' = [\theta_r, \theta_s, \alpha, n]$ were estimated for the MVG model, and three additional parameters (α^*, n^*, ω) were estimated for the DP model.

Test Site

All measurements were performed at the TERENO test site Selhausen, which is located in the river Rur catchment (North Rhine Westphalia, Germany). The underlying sediments are Quaternary sediments, which are mostly fluvial deposits from the Rhine/Meuse river and the Rur river system, covered by eolian sediments (up to a depth of 1 m) from the Pleistocene and Holocene. The major soil type is silty loam according to the USDA textural classification. The ground water depth shows seasonal fluctuations between 3-m and 5-m below the surface. A detailed description of the test site is given by Scharnagl et al. (2011) and Bauer et al. (2011).

Near the GPR setup, ten 100-cm^3 undisturbed soil samples were collected at each A and B horizon to determine the actual water retention curve and saturated hydraulic conductivity of the soil. Direct measurements were made with a sand box and pressure plate apparatus to provide the retention curve in the suction range 0 to 15000 cm. Low pressure heads were measured using the hanging water column technique (h < 100 cm), while high pressures heads were measured using the pressure cell extractor, and K_s was estimated using constant pressure head (Richards, 1948; Gee et al., 2002).

Experimental Setup

The stepped-frequency continuous-wave radar system was set up using a vector network analyzer (ZVL3, Rohde & Schwarz, Munich, Germany), with a monostatic antenna, thereby setting up an air-launched radar. The antenna system consisted of a linearly polarized, double-ridged broadband horn antenna (BBHA 9120 F, Schwarzbeck Mess-Elektronik, Schönau, Germany). The length of the antenna is 96 cm and its aperture area is 68 × 95 cm^2. The antenna nominal frequency range is 0.2 to 2.0 GHz and its isotropic gain ranges from 6 to 18 dBi. The high directivity of the antenna (45°3-dB beam width in both in E-plane and the H-plane at 1 GHz) makes it suitable for using off the ground. Measurements were performed with the antenna aperture situated at about 110 cm above the soil surface.

The antenna was connected to the reflection port of the ZVL3 via a high quality N-type 50-Ohm coaxial cable. During measurements the ZVL3 was calibrated daily at the connection between the antenna feed point and the cable using an Open-Short-Match calibration kit. The frequency dependent complex ratio S_{11} between the returned signal and the emitted signal was measured sequentially at 901 stepped operating frequencies over the range 200–2000 MHz with a frequency step of 2 MHz. To reduce the surface roughness effect, the lower frequency range of 200–800 MHz, was considered for the inversions. Furthermore,

the signal-to-noise ratio in the higher frequency range was lower due to a higher return loss and lower gain (Jadoon et al., 2010). TDR measurements were made using 3-rod probes of 30 cm length (CS605-L, Campbell Scientific Inc., Logan, Utah, USA) connected to a Campbell TDR100 system, SDMX50 coaxial multiplexer, and a CR3000 data logger.

The experiment was conducted on a bare agricultural field. Figure 2a and 2b, respectively, show the fully automated GPR experimental setup and the trench with TDR probes installed at 1.5-m distance from the footprint of the GPR antenna. In Fig. 2a, the double ridged horn antenna was fixed at 110 cm above the ground, as mentioned above, and the bare-soil surface was fully exposed to the natural processes, i.e., precipitation and evaporation. The vector network analyzer ZVL3 was placed in a box to protect it from rain and the sun. On one side of the GPR setup, TDR probes were installed horizontally in a trench at 8-, 15-, 20-, and 30-cm depth with two replicates, to monitor the lateral and vertical dynamics of the soil water content. It has to be noted that the TDR probes installed at 8 and 20 cm were 1 m apart from each other, whereas the pairs of probes at 15 and 30 cm were 0.5 m apart (see Fig. 2b). One additional TDR probe was installed at 60-cm depth. The trench was filled in after the installation of TDR probes. Time-lapse GPR and TDR measurements were performed to monitor the soil water flow dynamics. Data acquisition was computer-controlled and entirely automated over a twenty-day measurement period. The test site was equipped with a continuous electric supply and during measurements an uninterruptible power supply was provided to the GPR and TDR systems.

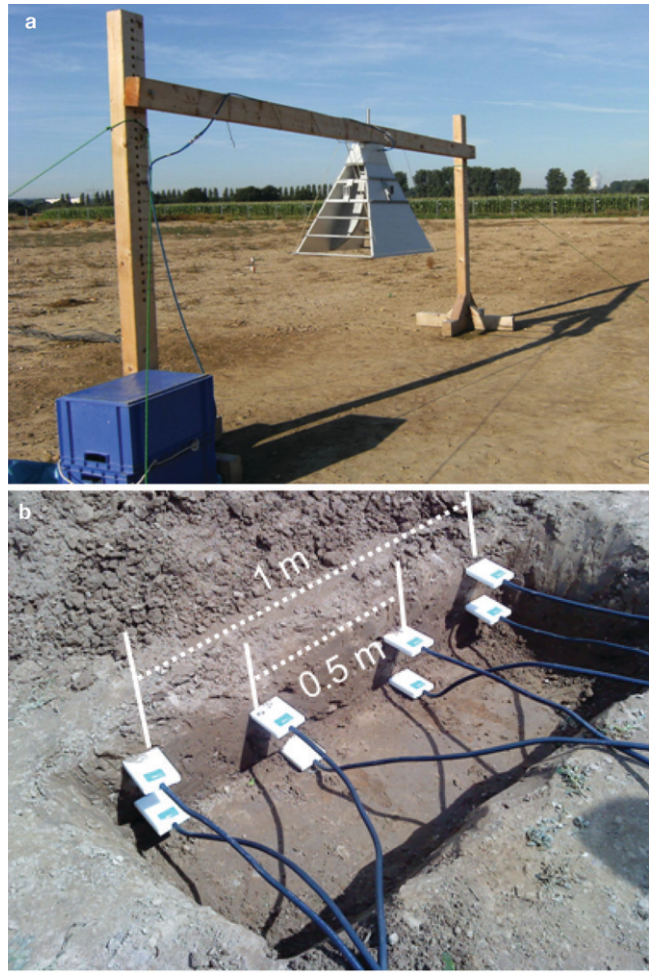

Fig. 2. (a) Fully automated ground-penetrating radar (GPR) setup with the antenna fixed at 110 cm above the ground. In (b) near the footprint of the GPR antenna, four pairs of time domain reflectometry (TDR) probes were installed in a trench to monitor the vertical dynamics and lateral variability of soil water content.

Results and Discussion

Ground-Truth Measurements

Figure 3 depicts the hourly observations of precipitation and potential evaporation (E_{pot}). The gray patch shows the 10-d period used for the spin-up of the hydrological model to minimize uncertainty in the initial conditions. In practical applications, the depth-dependent initial conditions in the hydrodynamic model are poorly known or not known at all. The width of the spin-up or adjustment periods is not well defined, but in practice it occurs rather fast (1–2 d) for most atmospheric fields (de Elia et al., 2002), but it may be much longer for some land-surface processes (such as deep soil hydrology). The spin-up time appears to depend on the soil type, the top boundary condition (precipitation and evaporation flux), and lower boundary condition considered at the time of initialization (Cosgrove et al., 2003; Laprise, 2008; Jadoon et al., 2008). The hydrological model undergoes a period of spin-up during which soil water content profiles adjust from the arbitrary initial conditions (t = 0), to an equilibrium state.

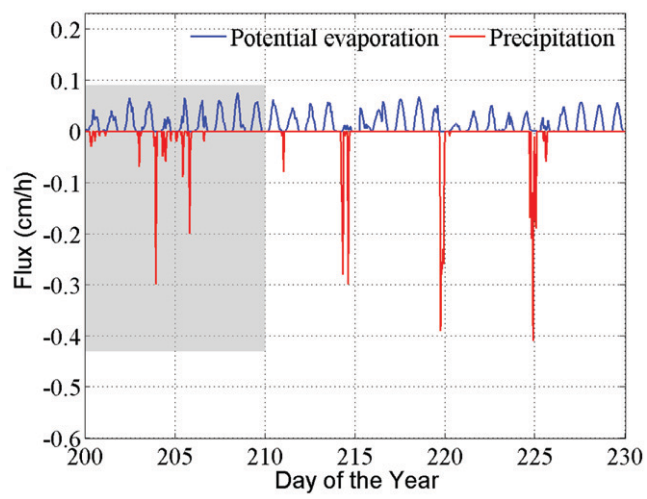

Fig. 3. Precipitation and potential evaporation flux values recorded over thirty-day period (meterological station at Selhausen, Germany). The gray patch represents the spin-up time to estimate initial conditions in the soil hydrodynamic model.

Precipitation and other meteorological variables were recorded at a meteorological station located 100 m west of the measurement site. Potential evaporation was estimated using the FAO-56 method

(Allen et al., 1998). The FAO-56 Penman–Monteith equation has two advantages over several existing evapotranspiration methods. First of all, it is a predominately physically based approach, indicating that the method can be used globally without any need for additional parameter estimations. The method requires air temperature, wind speed, relative humidity, and solar radiation data. Second, the method has been tested using a variety of lysimeters (Droogers and Allen, 2002). The FAO-56 method consists of two steps. First, the potential evapotranspiration from a grass reference surface, ET_{ref}, is calculated using a modified Penman–Monteith equation (Allen et al. (1998), p. 74). We used hourly averaged values of air temperature, relative humidity, wind speed, incoming shortwave radiation, and atmospheric pressure as input variables. In a second step, the reference evapotranspiration is scaled with an empirical coefficient, $E_{pot} = 1.15ET_{ref}$ (Allen et al. (1998). This coefficient reflects the increased evaporation potential of bare soils (as compared to the reference grass surface), which is mainly due to the lower albedo of wet soil surfaces.

Figure 4 shows the water content recorded by each pair of TDR probes installed at 8-, 15-, 20-, and 30-cm depths for the 20-d period, during which all TDR measurements were performed every 8 h. Lateral variations of 2 to 7% in water content were observed for TDR probes installed at 8- and 20-cm depth, which is partly explained by these probes being installed 1 m apart (see Fig. 2b). On the other hand, minor lateral variations in water content were recorded by the pair of TDR probes installed at 15 and 30 cm as the distance between the pair was only 0.5 m. Three precipitation events were clearly observed by all TDR probes up to a depth of 30 cm. On the other hand, soil water content measured at 60-cm depth showed nearly constant values (not shown). Additionally, fluctuation in water content at 60-cm depth was within the range of TDR measurement error, which is 0–2% (Bilskie, 1997). In the hydrodynamic model, the initial conditions were specified in terms of water content, and the lower boundary condition was considered as a constant water content fixed to the mean value of water content observed by TDR at 60-cm depth.

To estimate the field-specific parameters for the Rhoades model, 24 TDR readings were picked randomly at various depths between 5- and 60-cm depth. The apparent relative permittivity was inferred from the travel time of the TDR signal and translated to water content using Topp's equation (Eq. [6]), whereas the bulk soil electrical conductivity was inferred from the signal attenuation. For the latter, we used the reflection coefficient at late times, which is related to the load resistance according to Giese and Tiemann

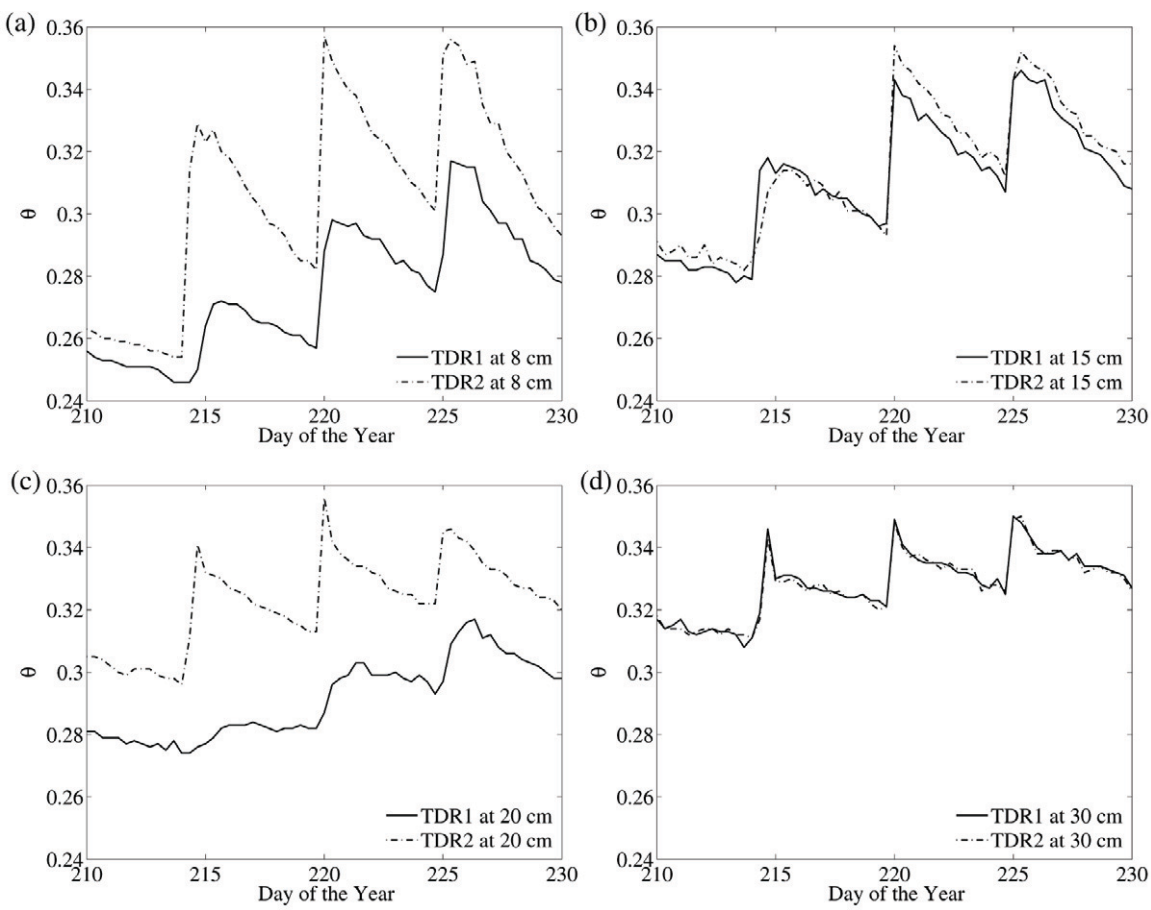

Fig. 4. Water content (θ) monitored by two time domain reflectometry (TDR) probes (solid and dash-dot lines) installed at each depth (8, 15, 20, 30 cm), with 8 h interval for a period of 20 days.

(1975). The load resistance can be translated to bulk electrical conductivity by applying the series resistor model (Heimovaara et al., 1995). Before collecting the field data, the series resistor model was calibrated for our setup following the two-step approach proposed by Huisman et al. (2008) and using eight aqueous solutions with different electrical conductivities. As recently shown by Bechtold et al. (2010), the TDR100 device is prone to measurement errors in the presence of polarization at the TDR probe rods when using the wrong waveform acquisition parameters. We accounted for this issue by applying the suggested minimum number of waveform averages and waveform data points during calibration and acquisition of the field data.

Figure 5 shows the Rhoades model fit to the measured bulk electrical conductivity and water content. The parameters A, B, and σ_s in Eq. [8] were estimated by inversion, whereby the parameter space was set relatively large, covering the whole range of values obtained by Rhoades et al. (1990), namely $10^{-4} < A < 1$ (Sm^{-1}), $-1 \times 10{-2} < B < 5 \times 10^{-4}$ (Sm^{-1}), and $5 \times 10{-5} < \sigma_s < 5.5 \times 10{-3}$ (Sm^{-1}). The optimal parameters retrieved for A, B, and σ_s were 0.1657, −0.0054, and 0.0041 (S m^{-1}), respectively. The fairly good fit of the Rhoades model to the field data justifies the use of a single petrophysical parameter set for the whole soil profile.

Time-Lapse Green's Function

Figure 6 shows the measured time-lapse Green's function in frequency-domain (amplitude 6a, and phase 6b, and in time-domain 6c. Precipitation and evaporation data are plotted on top of the measured amplitude of the Green's function to visualize the effect of the atmospheric boundary conditions on the radar data. Radar signals were recorded with a constant time-step of 10 min for 20 days, resulting in a total 2880 measurements. As already stated, three major precipitation events occurred during the measurement period and can be visually observed in the amplitude of the Green's function in both the frequency and time domain. At the time of precipitation the amplitude of the Green's function increases due to the strong reflection at the wet soil surface, and vice versa for dry soil surface. This response can be observed especially in the amplitude of the surface reflection in the time-domain Green's function, which is sensitive to shallow subsurface dynamics. A similar response was observed in the amplitude of the frequency-domain Green's function at high frequencies. The frequency-domain Green's function has more information as compared to the time-domain Green's function. For instance,

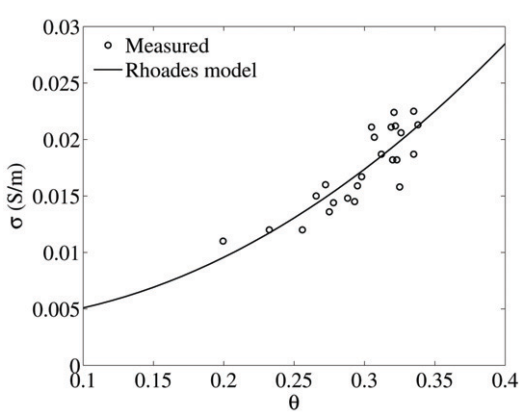

Fig. 5. The soil electrical conductivity (σ) obtained from time domain reflectometry (TDR) measurements as a function of TDR derived water content (θ) using Topp's model, and the Rhoades model was fitted to the σ and θ data.

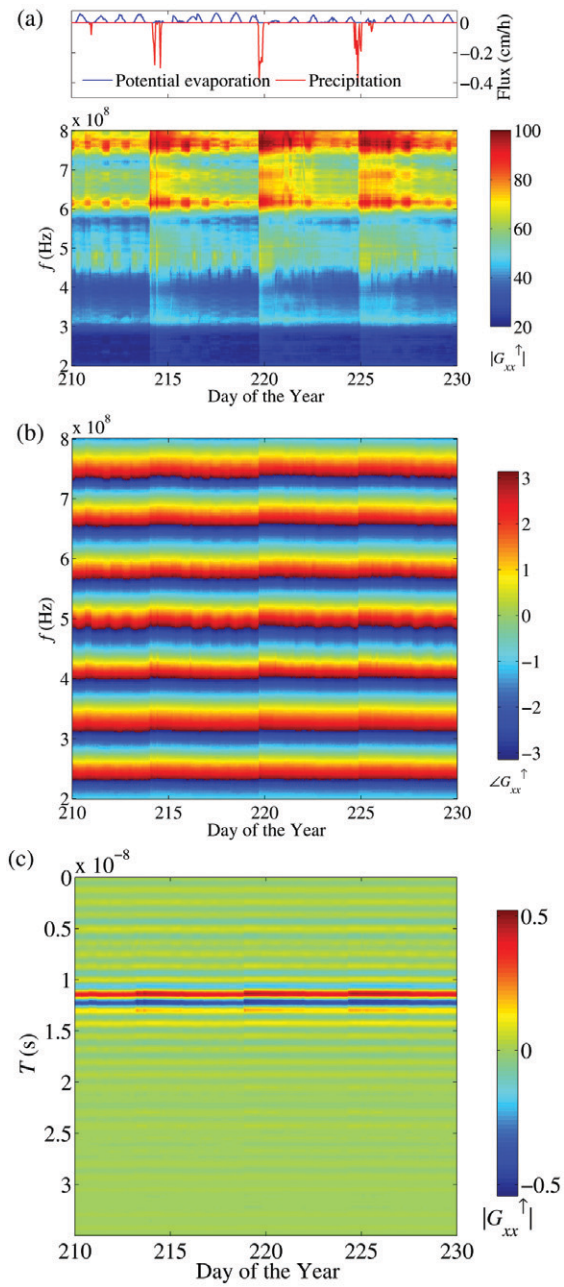

Fig. 6. Measured time-lapse Green's function in the frequency domain (dimensionless), (a) $\left|G_{xx}^{\uparrow}\right|$ denotes the amplitude, (b) $\angle G_{xx}^{\uparrow}$ denotes the phase of the Green's function and (c) depicts the time-domain Green's function. Frequency is denoted by f and T is the two-way travel time. Precipitation and potential evaporation fluxes are plotted on the top of the measured amplitude of the Green's function. Time-lapse radar data were recorded for twenty days with a 10-min time step.

before the first precipitation event, evaporation fluxes were observed for 4 d, and this effect can be noticed by relatively weak reflection amplitude of the time-lapse Green's function at 600–800 MHz. At night, the evaporation flux is very low and a slight increase in the surface moisture occurs, most likely due to dew, whereby this effect can be noticed at high frequencies after consecutive evaporation events. On the other hand, low frequencies of the radar signal are sensitive to greater depths. Such an effect cannot be visually observed in the time-lapse Green's function. TDR data indicates that the soil water content dynamics decreased with depth. Therefore, only slight variations can be observed in the amplitude of Green's function in the 200–300 MHz frequency range. In the phase of the time-lapse Green's function a slight shift can be noticed due to precipitation events. The effect of the soil water content dynamics can be better visualized in the amplitude as compared to the phase of the time-lapse Green's function in the frequency-domain. Jadoon et al. (2010) analyzed the same dataset in the time-domain to estimate the variation of surface soil water content.

The saturated water content θ_s for the top layer was estimated from the radar data acquired just after the three major precipitation events, assuming saturation of the top few centimeters of the soil (Jadoon et al., 2010), whereby inversion of the radar signal was performed in the time domain, focusing on the surface reflection only (Lambot et al., 2006c). The radar signal was inverted assuming unknown antenna height and unknown soil dielectric permittivity. The mean of the three water contents obtained just after the three major precipitation events was 0.426 ($cm^3\ cm^{-3}$), which is in good agreement with the value measured on undisturbed soil samples [0.412 ($cm^3\ cm^{-3}$)] (Jadoon et al., 2010). The residual water content θ_r could not be estimated from the measured radar data as the top few centimeters of the soil never fully dried. The minimum soil water content observed by Jadoon et al. (2010) was 0.18 ($cm^3\ cm^{-3}$). As a consequence, in the hydrogeophysical inversion, and θ_s and θ_r were fixed to 0.426 ($cm^3\ cm^{-}$) and 0.045 ($cm^3\ cm^{-3}$). The value of θ_r was taken from laboratory data. In a previous study, Lambot et al. (2009) estimated both the θ_s and θ_r independently from the off-ground GPR measurements in a fully saturated and dry condition, respectively.

Figure 7 depicts the measured and modeled (fitted) time-lapse, frequency- and time-domain Green's functions. To minimize computation time for the integrated full-waveform inversion, a total of 15 GPR observations were selected, each to catch most of the observed dynamics. The general behavior of the measured Green's function is relatively well reproduced by the modeled Green's functions (see Fig. 7a–7i), in particular, the variation range for the amplitude is similar (the same color scale was used for all plots). This agreement can be partly attributed to the fact that the saturated water content was fixed and estimated from the radar data. The phase of the measured and modeled Green's functions are almost the same. It is worth nothing that the effects of the three precipitation events are clearly visible in the modeled Green's functions.

Figure 7d and 7e show the amplitude and phase of the modeled Green's function obtained by the full-waveform hydrogeophysical inversion of time-lapse GPR data by using MVG model for both A and B horizons, whereby six soil hydraulic parameters were retrieved by the modeled Green's function. The estimated soil hydraulic parameters are listed in the column named GPR MVG inversion in Table 1 and fixed parameters are marked with superscript ‡. The amplitude of the modeled Green's function matches the amplitude of the measured radar data best at low frequencies. In another inversion, the A and B horizon was considered as a dual and single porosity system, respectively, and nine parameters were inversely estimated. The modeled amplitude and phase of the Green's function for this setup are depicted in Fig. 7g and 7h. At the higher frequency range 600–800 MHz, the modeled amplitude of the Green's function obtained by the dual-porosity model (Fig. 7g) better matches the measured amplitude, as compared to the modeled amplitude of the Green's function by using the MVG model (Fig. 7c). The results of the modeled Green's functions showed that the DP model can better explain the soil water dynamics at shallow depths as compared to the MVG model. The stopping criterion for the inversion was specified with respect to the convergence criterion in which an optimum was assumed to be reached when the objective function did not improve by more than 0.01% in 20 successive evolution loops. The calculation of these full-waveform hydrogeophysical inversions required 35 to 55 h of computational time in MATLAB using a 1.7 MHz laptop with 2 GB of RAM. The difference in smoothness between the observed and predicted datasets may be attributed to the assumption of one-dimensional water flow, the assumed homogenous soil layers, frequency and temperature independence of the petrophysical relationships, and partly to the measurement errors, e.g., small ringing effects can be observed at 5 ns in the measured time-domain data (Fig. 7c), which cannot be visualized in the modeled signals (Fig. 7f and 7i). The next logical step is to test the proposed approach on a large scale and do time-lapse GPR measurements on a grid plot. Statistical analysis will be performed to determine how many measurements should be needed before and after the precipitation events to precisely estimate the soil hydraulic parameters. Furthermore, the uncertainty will be analyzed with respect to the hydraulic parameters of the DP and MVG models in the integrated hydrogeophysical inversion of time-lapse GPR data.

Water Retention and Hydraulic Conductivity Functions

Figure 8 depicts the water retention and hydraulic conductivity curves for the A and B horizons. The red circular markers show the mean of the ten retention datasets for the undisturbed soil samples collected at each horizon and the bar shows the maximum and minimum retention data at each pressure step. The mean saturated hydraulic conductivity, K_s, estimated from ten soil samples was

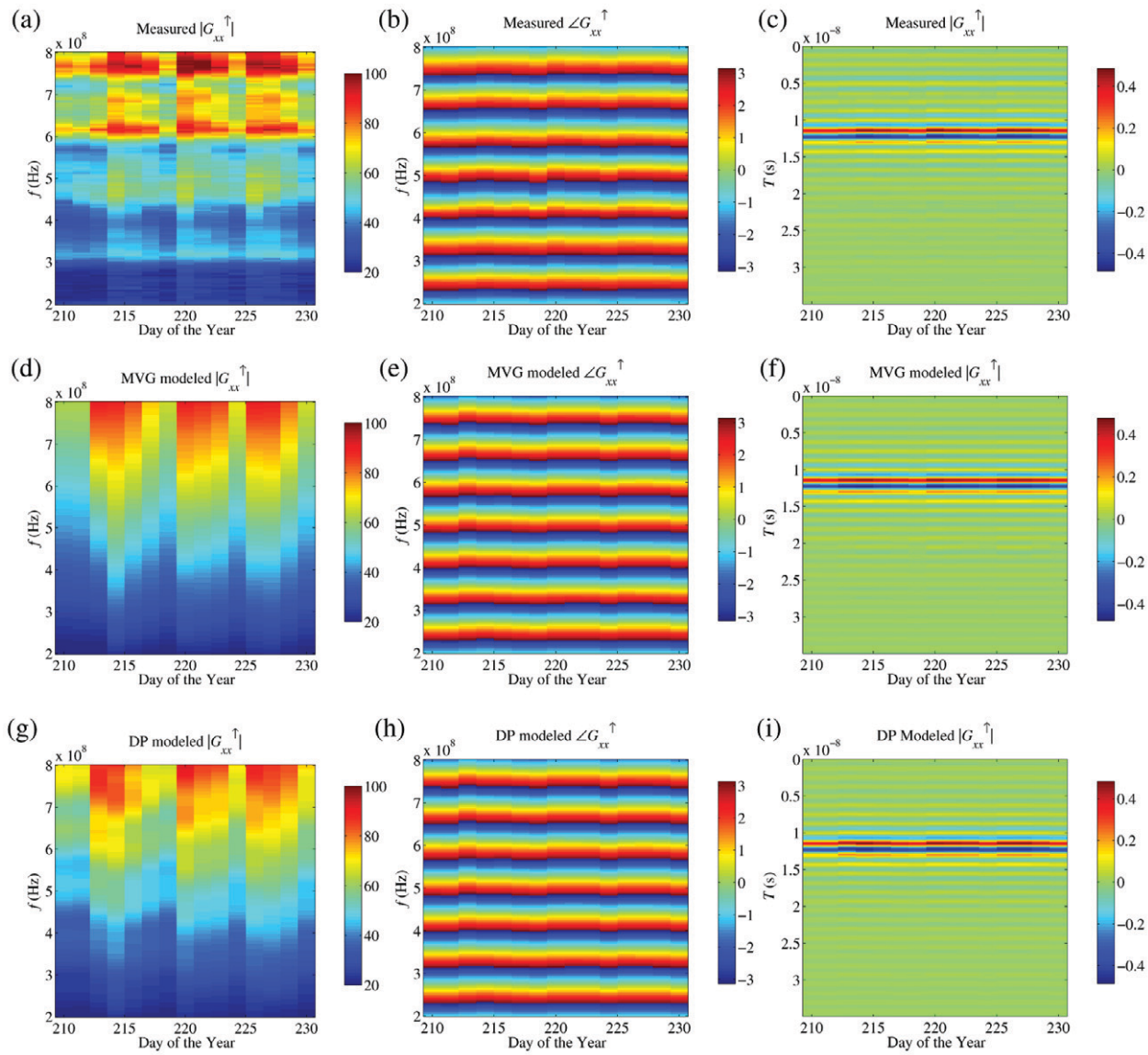

Fig. 7. Measured and modeled time-lapse Green's functions in the time domain and frequency domain (dimensionless), $\left|G_{xx}^{\uparrow}\right|$ denotes the amplitude and $\left|G_{xx}^{\uparrow}\right|$ denotes the phase, f is the frequency, T is the two-way travel time. Fifteen time-lapse radar measurements were considered to reconstruct modeled Green's function by using Mualem–van Genuchten (MVG) and dual porosity (DP) models in hydrogeophysical inversion of time-lapse GPR data.

20.61 and 23.87 (cm h^{-1}), respectively, for the A and B horizon. For the direct characterization from the collected samples, the MVG and dual porosity models were fitted by formulating an unweighted least-squares problem using the SCE-UA optimization algorithm. In total, four inversions were performed for undisturbed soil samples. Two inversions for each A and B horizon were performed, by considering a single and dual porosity system for each horizon. In the inversion for the undisturbed soil samples, the parameter λ was fixed to 0.5, K_s was fixed to the mean value estimated from soil samples, and the remaining parameters for the MVG and DP models were estimated by inversion. To generate the modeled MVG and DP retention curve, Eq. [3] was used and fitted to the red circular markers to estimate the hydraulic parameters from the undisturbed soil samples. The hydraulic parameters obtained for the soil samples are depicted in Table 1. The inversion stopping criterion was fixed to the convergence criterion in which an optimal was assumed to be reached when the objective function did not improve by more than 0.001% in 20 successive evolution loops and inversion was completed in 2 min. The DP model curve fits the data of the undisturbed soil samples well, which clearly indicates macro-porosity close to saturation. In the water retention curve (Fig. 8c), the second layer has smaller error bars, which denotes less spatial soil heterogeneity as compared to the top soil layer.

In Fig. 8a and 8b, the estimated water retention and hydraulic conductivity curves from the time-lapse GPR data are shown by red-dashed and black lines, respectively, for the GPR inversion

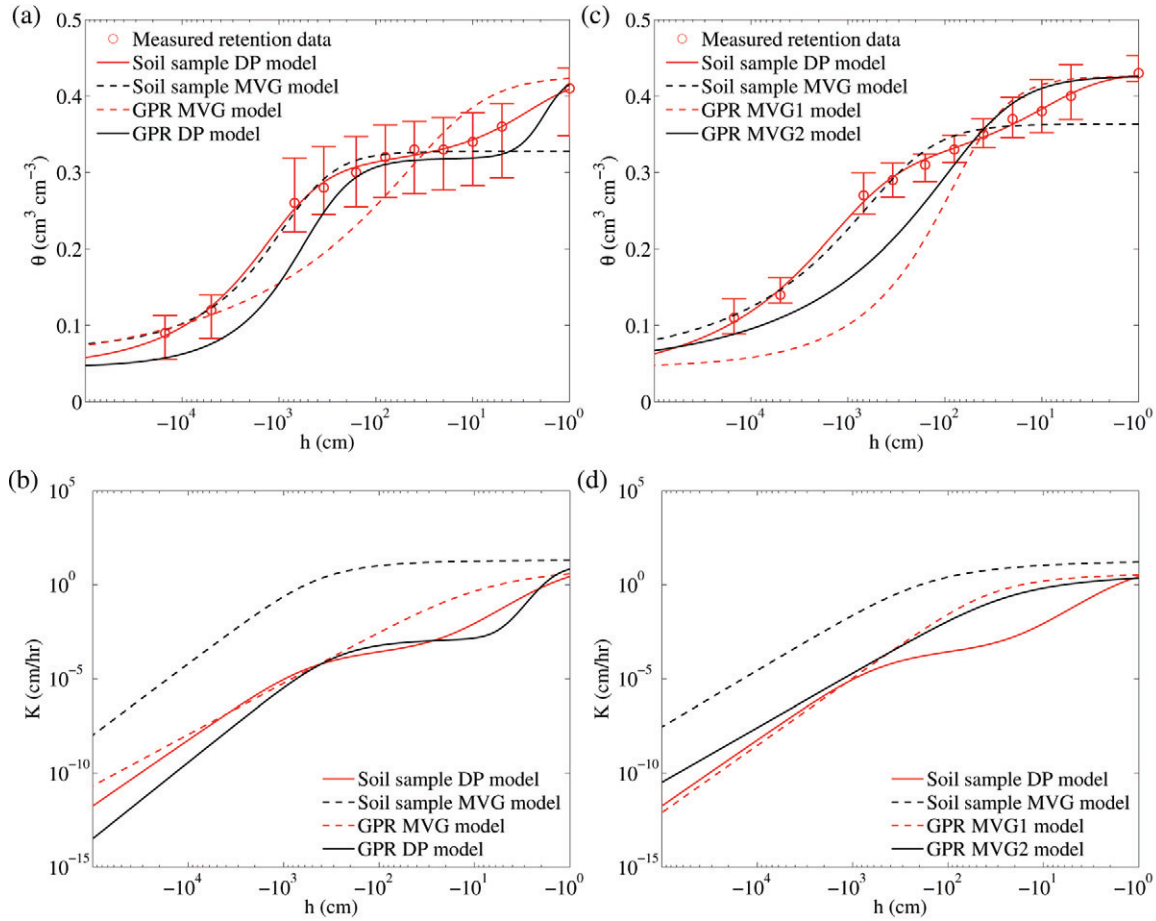

Fig. 8. Water retention and hydraulic conductivity as a function of pressure head estimated from mean of reference data (red circular markers) and integrated hydrogeophysical inversion of time-lapse ground-penetrating radar (GPR) data for A and B horizon, respectively, (a,b) and (c,d). The bars show the maximum and minimum retention values for ten undisturbed soil samples collected at each A and B horizon. In Fig. 8 (c,d), GPR MVG1 and GPR MVG2, respectively, corresponds to B horizon when MVG and DP models were used for A horizon in the time-lapse hydrgeophysical inversion.

using the MVG and DP models. The classical MVG model was used for both layers in the first inversion of time-lapse radar data to estimate α, n, and K_s for each layer. In the second inversion, the first layer was considered as a dual porosity system and the second layer as a single porosity system. In total nine parameters were estimated: six for the first layer (α, n, K_s, α^*, n^*, and ω^*) and three for the second layer (α, n, and K_s). The estimated values are listed in Table 1. The retention curves obtained by the DP inversion of time-lapse GPR data are more realistic and their shape agrees quite well with the curves obtained from undisturbed soil samples Fig. 8a.

The saturated hydraulic conductivity K_s estimated by integrated hydrogeophysical inversion of radar data is underestimated compared to the undisturbed soil samples characterization (see Table 1). As emphasized by Schaap and Leij (2000) and in particular argued by Van Genuchten and Nielsen (1985) and Luckner et al. (1989), K_s may not be an especially suitable matching point because K_s is essentially sensitive to the flow in the larger pores (it is not meant here preferential flow), whereas unsaturated flow occurs in significantly smaller pores. A matching point at slightly unsaturated conditions (defining a K_0) would yield better results to predict unsaturated flows using the unimodel Mualem-van Genuchten model (Weynants et al., 2009). In that respect, the inversion of the radar data is expected to provide such K_0 instead of the real K_s. It should be emphasized that hydrodynamic inverse modeling provides so-called effective parameters in terms of the hydrodynamic observations, and these parameters are typically different from the undisturbed soil sample (direct characterization). Such discrepancies usually originate from the different characterization scales (the hydraulic properties of a soil are not homogeneous) and hydrodynamic phenomena that may not be taken into account in the model (e.g., air entrapment, hydrophobicity, preferential flow, and hysteresis). Finally, the non-perfect lateral homogeneity of the soil as observed by the TDR measured water content at the same depth may also explain a part of the observed discrepancies.

This research has not directly addressed the challenges with respect to the spatial soil heterogeneity and the corresponding model errors that may occur when it is not taken into account, potentially biasing hydraulic parameter estimates obtained in hydrogeophysical inversion. Spatial variations in soil moisture may result from changes in soil texture rather than flow. Local change in water

content can also be produced by soil layering, which affects both the water retention and soil hydraulic conductivity. Soil heterogeneity and the related phenomena have not been taken into account in the one-dimensional model. In addition, errors in the estimates of potential evaporation and errors in the calibration of petrophysical relationships at the field scale may be challenging in the context of coupled hydrogeophysical inversion.

Water Content Profiles

Figure 9a–9c shows the HYDRUS 1-D computed water content profiles based on the hydraulic parameters obtained from undisturbed soil samples, time-lapse GPR inversion for MVG model parameters, and time-lapse GPR inversion for DP model parameters, respectively. The top boundary condition was considered as a time-variable flux, including real precipitation and potential evaporation data and the lower boundary was considered as constant water content. In total, 60 water content profiles were reconstructed with a time-step of 8 h to compare the water content obtained at 8-, 15-, 20-, and 30-cm depth with the TDR measured water content at these depths (see Fig. 10). In all cases, the effect of the three precipitation events can be clearly observed. The wetting front after the first precipitation event can be visualized in Fig. 10a–10c and after all precipitation events a propagating drying front can be observed due to ongoing evaporation, especially in the dual porosity cases. Irrespective of the rainfall events, variations in water content in the bottom layer (32–60 cm) are small. A clear difference in water content can be observed at 32-cm depth, which separates the top from the bottom layer. Water content profiles obtained from the time-lapse radar inversion with a DP model for the first layer corresponds well to the water content profiles obtained from undisturbed soil samples (see Fig. 9a and 9c), especially at shallow depths and after each precipitation event. In Fig. 9b, higher water content can be observed in the top few centimeters as compared to DP water content profiles.

For a better visualization of the goodness of fit of the hydraulic parameters, Fig. 10a and 10b show the soil water content derived from the hydrogeophysical inversion of time-lapse GPR data using the MVG and DP models, respectively, plotted with respect to the TDR derived water content at the four measurement depths. It has to be noted that only the mean of the TDR replicates for each depth was considered. From Fig. 10a, it can be seen that GPR-derived water contents significantly underestimate the TDR measurements if the MVG parameterization is used in the hydrological model. Additionally, the data points are scattered, resulting in a relatively low correlation coefficient (r^2 = 0.69) and a root mean square error (RMSE) in terms of water content of 0.017 ($cm^3\ cm^{-3}$). The observed discrepancies are similar for all four depths, whereby GPR derived volumetric water content at 15-cm depth shows the largest systematical underestimation. The soil water content underestimation may be attributed to the single porosity system considered for both layers. In additional, the misfit of the regression line compared with the 1:1 line is most pronounced for larger water contents. The

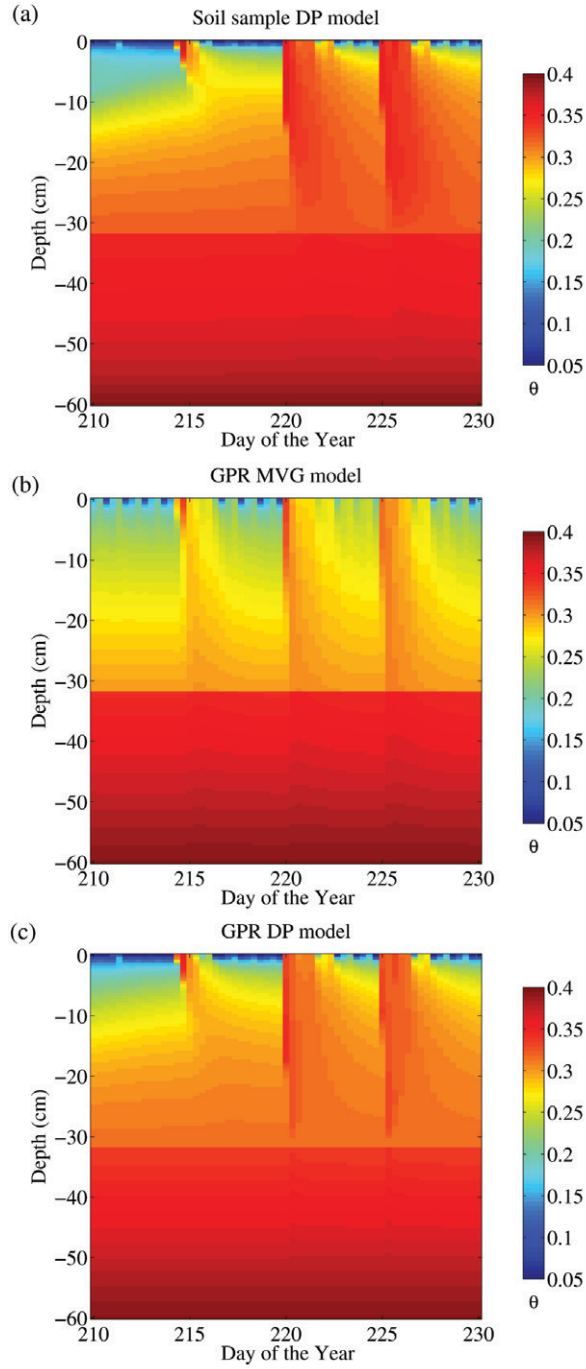

Fig. 9. Volumetric water content θ as a function of depth and time in days of the year, obtained from the hydrodynamic modeling (a) dual porosity (DP) model parameters obtained from undisturbed soil samples, (b) Mualem–van Genuchten (MVG) model parameters inferred by time-lapse ground-penetrating radar (GPR) inversion, and (c) DP model parameters estimated from time-lapse GPR inversion.

comparison of soil water content estimated from the time-lapse GPR inversion using DP model and TDR data is shown in Fig. 10b with less scattering, and therefore, a higher r^2 of 0.79 and a lower RMSE of 0.010 ($cm^3\ cm^{-3}$). In the high water content range, the GPR-derived water contents underestimate the TDR measurements also when using the DP model. Water content estimated using the DP

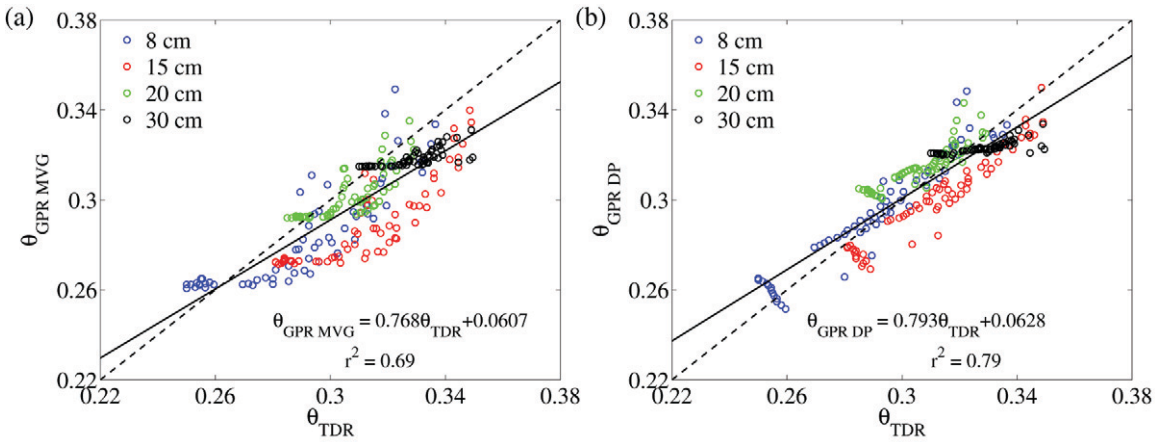

Fig. 10. Soil water content at four depths (8, 15, 20, and 30) cm obtained from hydrodynamic modeling using (a) Mualem-van Genuchten (MVG) and (b) dual porosity (DP) model in the hydrogeophysical inversion versus TDR inferred water content.

model are less scattered as compared to the MVG model used in the integrated hydrogeophysical inversion.

Conclusions

Integrated full-waveform electromagnetic and one-dimensional vertical hydrodynamic inversion of time-lapse GPR data was used to infer the shallow unsaturated soil hydraulic parameters of a two-layer soil model from a dataset collected at a fixed location in a bare agricultural field. The radar antenna was air-launched and the surface of soil was fully exposed to natural conditions, i.e., evaporation and precipitation events. In GPR data processing, a relatively low-frequency range (200–800 MHz) was used to avoid surface roughness effects, which were not accounted for by the electromagnetic model. The effect of the evaporation and three major precipitation events were well captured in measured full-waveform time-lapse GPR data in frequency- and time-domain. It was shown that at the time of precipitation the amplitude of the both frequency- and time-domain increases due to strong reflection at the wet soil surface, and vice versa for the dry soil surface. In addition, the effect of the evaporation can be visually noticed in the amplitude of the frequency-domain at high frequencies.

At the test site macroscopic observations and the retention data obtained from undisturbed soil samples are evidence for the dual-porosity character of the soil. As a consequence, both single and dual porosity models were tested in the integrated hydrogeophysical inversion of time-lapse GPR data. Parameters of the water retention and hydraulic conductivity functions are better predicted by using dual porosity model in the hydrogeophysical inversion rather than the single porosity model. Furthermore, the dual porosity model fits well to the retention data obtained from the undisturbed soil samples. The improvement with the dual porosity model could also be observed in the comparison of modeled water content and independently measured soil water content from TDR. The comparison with the soil hydraulic properties determined from the undisturbed soil samples using standard laboratory methods indicates that the soil hydraulic parameters estimated by integrated hydrogeophysical inversion present plausible values. Such differences usually originate from the different characterization scales. Resulting parameters can be considered as effective parameters that best describe the soil water content dynamics in the field.

The results represent a promising step toward application of the approach for noninvasive characterization of the shallow soil properties at the field scale. The major challenge at the field scale will be to keep the number of fitting parameters low. For sufficiently long time spans, the spatial variability of θ_s and θ_r can be directly inferred from the GPR data at very wet and dry conditions, respectively. A conceptual model of a two-layer system with a uniform thickness of the first layer might be applicable for many agricultural fields with a plow horizon. We believe that the major remaining issue of the application at the field scale will be the spatial soil heterogeneity and variability of the petrophysical properties and how it affects the estimates of the hydraulic properties when assuming the petrophysical properties to be spatially uniform.

Acknowledgments

This work was supported by the Forschungszentrum Jülich GmbH (Germany), the Université catholique de Louvain and Fonds National de la Recherche Scientifique (UCL and FNRS, Belgium). Khan Zaib Jadoon was funded by the CROPSENSe project funded by Bundesministerium für Bildung und Forschung (BMBF, Germany). Support for Susan Hubbard and Michael Kowalsky was provided by DOE Contract DE-AC0205CH11231 to LBNL. The authors are grateful to Marc Grasmueck, two anonymous reviewers, and the associate editor for their efforts in improving the manuscript.

References

Allen, R.G., L.S. Pereira, D. Raes, and M. Smith. 1998. Crop evapotranspiration-Guidelines for computing crop water requirements. FAO Irrigation and Drainage Paper No. 56. Rome, Italy.

Archie, G.E. 1942. The electrical resistivity log as an aid in determining some reservoir characteristics. Trans. Am. Inst. Min. Metal. Eng. 146:54–61.

Assouline, S., D. Tessier, and A. Bruand. 1998. A conceptual model of the soil water retention curve. Water Resour. Res. 34(2):223–231. doi:10.1029/97WR03039

Bauer, J., L. Weihermüller, J. Huisman, M. Herbst, A. Graf, J. Séquaris, and H. Vereecken. 2011. Inverse determination of heterotrophic soil respiration

response to temperature and water content under field conditions. Biogeochemistry 108(1–3):119–134. doi:10.1007/s10533–011–9583–1.

Bechtold, M., J.A. Huisman, L. Weihermüller, and H. Vereecken. 2010. Accurate determination of the bulk electrical conductivity with the TDR100 cable tester. Soil Sci. Soc. Am. J. 74(2):495–501. doi:10.2136/sssaj2009.0247

Bilskie, J. 1997. Reducing measurement errors of selected soil water sensors. In M.T. van Genuchten and F.J. Leij, editors, Proceedings of the International workshop on characterization and measurement of the hydraulic properties of unsaturated porous media, Part 1. Riverside, CA. p. 387–396.

Binley, A., G. Cassiani, R. Middleton, and P. Winship. 2002a. Vadose zone flow model parameterisation using cross-borehole radar and resistivity imaging. J. Hydol. 267(3–4):147–159. doi:10.1016/S0022-1694(02)00146-4

Binley, A., P. Winship, L.J. West, M. Pokar, and R. Middleton. 2002b. Seasonal variation of moisture content in unsaturated sandstone inferred from borehole radar and resistivity profiles. J. Hydrol. 267(3–4):160–172. doi:10.1016/S0022-1694(02)00147-6

Bridge, B.J., J. Sabburg, K.O. Habash, J.A.R. Ball, and N.H. Hancock. 1996. The dielectric behaviour of clay soils and its application to time domain reflectometry. Aust. J. Soil Res. 34(6):825–835. doi:10.1071/SR9960825

Cassiani, G., and A. Binley. 2005. Modeling unsaturated flow in a layered formation under quasi-steady state conditions using geophysical data constraints. Adv. Water Res. 28(5):467–477. doi:10.1016/j.advwatres.2004.12.007

Cosgrove, B.A., D. Lohmann, K.E. Mitchell, P.R. Houser, E.F. Wood, J. C. Schaake, A. Robock, J. Sheffield, Q.Y. Duan, L.F. Luo, R.W. Higgins, R.T. Pinker, and J.D. Tarpley. 2003. Land surface model spin-up behavior in the North American land data assimilation system (NLDAS). J. Geophys. Res. Atmos. 108(D22): 8845–8864. doi:10.1029/2002jd003316.

Davis, J.L., and A.P. Annan. 1989. Ground penetrating radar for high resolution mapping of soil and rock stratigraphy. Geophys. Prospect. 37:531–551. doi:10.1111/j.1365-2478.1989.tb02221.x

de Elia, R., R. Laprise, and B. Denis. 2002. Forecasting skill limits of nested, limited area models: A perfect model approach. Monthly Weather Rev. 130(8):2006–2023. doi:10.1175/1520–0493(2002)130

Droogers, P., and R.G. Allen. 2002. Estimating reference evapotranspiration under inaccurate data conditions. Irrig. Drain. Syst. 16(1):33–45. doi:10.1023/A:1015508322413

Duan, Q.Y., S. Sorooshian, and V. Gupta. 1992. Effective and efficient global optimization for conceptual rainfall-runoff models. Water Resour. Res. 28(4):1015–1031. doi:10.1029/91WR02985

Durner, W. 1994. Hydraulic conductivity estimation for soils with heterogeneous pore structure. Water Resour. Res. 30(2):211–223. doi:10.1029/93WR02676

Fuentes, C., R. Haverkamp, and J.Y. Parlange. 1992. Parameter constraints on closed-form soil water relationships. J. Hydrol. 134:117–142. doi:10.1016/0022-1694(92)90032-Q

Gee, G.W., A.L. Ward, Z.F. Zhang, G.S. Campbell, and J. Mathison. 2002. The influence of hydraulic nonequilibrium on pressure plate data. Vadose Zone J. 1(1):172–178.

Gerke, H.H., and M.T. van Genuchten. 1993. A dual-porosity model for simulating the preferential movement of water and solutes in structured porous media. Water Resour. Res. 29(2):305–319. doi:10.1029/92WR02339

Ghose, R., and E.C. Slob. 2006. Quantitative integration of seismic and GPR reflections to derive unique estimates for water saturation and porosity in subsoil. Geophys. Res. Lett. 33(5):L05404.

Giese, K., and R. Tiemann. 1975. Determination of complex permittivity from thin-sample time domain reflectometry improved analysis of step response waveform. Adv. Mol. Relax. Proc. 7(1):45–59. doi:10.1016/0001-8716(75)80013-7

Giroux, B., E. Gloaguen, and M. Chouteau. 2007. Bhtomo a Matlab borehole georadar 2D tomography package. Comput. Geosci. 33(1):126–137. doi:10.1016/j.cageo.2006.05.014

Gloaguen, E., B. Giroux, D. Marcotte, and R. Dimitrakopoulos. 2007a. Pseudo full-waveform inversion of borehole GPR data using stochastic tomography. Geophysics 72(5): J43–J51. doi:10.1190/1.2755929

Gloaguen, E., D. Marcotte, B. Giroux, C. Dubreuil, Boisclair, M. Chouteau, and M. Aubertin. 2007b. Stochastic borehole radar velocity and attenuation tomographies using cokriging and cosimulation. J. Appl. Geophys. 62(2):141–157. doi:10.1016/j.jappgeo.2006.10.001

Grote, K., S.S. Hubbard, and Y. Rubin. 2003. Field scale estimation of volumetric water content using GPR ground wave techniques. Water Resour. Res. 39(11):1321–1335. doi:1310.1029/2003WR002,045.

Haarder, E.B., M.C. Looms, K.H. Jensen and L. Nielsen. 2011. Visualizing unsaturated flow phenomena using high resolution reflection ground penetrating radar. Vadose Zone J. 10(1):84–97. doi:10.2136/vzj2009.0188

Harter, T., and J.W. Hopmans. 2004. Role of vadose-zone flow processes in regional-scale hydrology: Review, opportunities and challenges. Unsaturated-Zone Modeling: Progress, Challenges and Applications, Vol. 6. Springer, Dordrecht.

Heimovaara, T.J., A.G. Focke, W. Bouten and J.M. Verstraten. 1995. Assessing temporal variations in soil water composition with time domain reflectometry. Soil Sci. Soc. Am. J. 59:689–698. doi:10.2136/sssaj1995.03615995005900030009x

Hinnell, A.C., T.P.A. Ferre, J.A. Vrugt, J.A. Huisman, S. Moysey, J. Rings, and M.B. Kowalsky. 2010. Improved extraction of hydrologic information from geophysical data through coupled hydrogeophysical inversion. Water Resour. Res. 46: W00D40.

Holliger, K., M. Musil, and H.R. Maurer. 2001. Ray-based amplitude tomography for crosshole georadar data: A numerical assessment. J. Appl. Geophys. 47:285–298. doi:10.1016/S0926-9851(01)00072-6

Hubbard, S.S., and Y. Rubin. 2000. Hydrogeological parameter estimation using geophysical data: A review of selected techniques. J. Contam. Hydrol. 45(1–2):3–34. doi:10.1016/S0169-7722(00)00117-0

Huisman, J.A., S.S. Hubbard, J.D. Redman, and A.P. Annan. 2003. Measuring soil water content with ground penetrating radar: A review. Vadose Zone J. 2:476–491.

Huisman, J.A., C.P. Lin, L. Weihermüller, and H. Vereecken. 2008. Accuracy of bulk electrical conductivity measurements with time domain reflectometry. Vadose Zone J. 7(2):426–433. doi:10.2136/vzj2007.0139

Huisman, J.A., J. Rings, J.A. Vrugt, J. Sorg and H. Vereecken. 2010. Hydraulic properties of a model dike from coupled bayesian and multi criteria hydrogeophysical inversion. J. Hydrol. 380(1–2):62–73. doi:10.1016/j.jhydrol.2009.10.023

Iden, S.C. and W. Durner. 2007. Free form estimation of the unsaturated soil hydraulic properties by inverse modeling using global optimization. Water Resour. Res. 43(7):W07451. doi:0.1029/2006WR005845.

Jacob, R.W. and J.F. Hermance. 2004. Assessing the precision of GPR velocity and vertical two-way travel time estimates. J. Environ. Eng. Geophys. 9(3):143–153. doi:10.4133/JEEG9.3.143

Jadoon, K.Z., E.C. Slob, M. Vanclooster, H. Vereecken, and S. Lambot. 2008. Uniqueness and stability analysis of hydrogeophysical inversion for time-lapse ground-penetrating radar estimates of shallow soil hydraulic properties. Water Resour. Res. 44:W09421. doi:10.1029/2007WR006639.

Jadoon, K.Z., S. Lambot, B. Scharnagl, J. van der Kruk, E. Slob, and H. Vereecken. 2010. Quantifying field-scale surface soil water content from proximal GPR signal inversion in the time domain. Near Surf. Geophys. 8(6):483–491.

Jadoon, K.Z., S. Lambot, E.C. Slob and H. Vereecken. 2011. Analysis of horn antenna transfer functions and phase-center position for modeling off-ground GPR. IEEE Trans. Geosci. Remote Sensing 49(5):1649–1662. doi:10.1109/TGRS.2010.2089691

Jonard, F., L. Weihermuller, K.Z. Jadoon, M. Schwank, H. Vereecken, and S. Lambot. 2011. Mapping field-scale soil moisture with L-band radiometer and ground-penetrating radar over bare soil. IEEE Trans. Geosci. Remote Sensing 49(8):2863–2875. doi:10.1109/TGRS.2011.2114890

Jonard, F., L. Weihermuller, H. Vereecken, and S. Lambot. 2012. Accounting for soil surface roughness in the inversion of ultrawideband off-ground GPR signal for soil moisture retrieval. Geophysics 77(1):H1– H7. doi:10.1190/geo2011-0054.1

Jones, S.B., and S.P. Friedman. 2000. Particle shape effects on the effective permittivity of anisotropic or isotropic media consisting of aligned or randomly oriented ellipsoidal particles. Water Resour. Res. 36(10):2821–2833. doi:10.1029/2000WR900198

Klotzsche, A., J. van der Kruk, G.A. Meles, J. Doetsch, H. Maurer, and N. Linde. 2010. Full-waveform inversion of cross-hole ground-penetrating radar data to characterize a gravel aquifer close to the Thur river, Switzerland. Near Surf. Geophys. 8(6):635–649.

Kool, J.B., J.C. Parker and M.T. van Genuchten. 1985. Determining soil hydraulic properties from one-step outflow experiments by parameter estimation: Theory and numerical studies. Soil Sci. Soc. Am. J. 49:1348–1354. doi:10.2136/sssaj1985.03615995004900060004x

Kowalsky, M.B., S. Finsterle, J. Peterson, S. Hubbard, Y. Rubin, E. Majer, A. Ward, and G. Gee. 2005. Estimation of field-scale soil hydraulic and dielectric parameters through joint inversion of GPR and hydrological data. Water Resour. Res. 41:W11425. doi:11,410.11,029/12,005WR004,237.

Kowalsky, M.B., J. Birkholzer, J. Peterson, S. Finsterle, S. Mukhopadhyay, and Y. Tsang. 2008. Sensitivity analysis for joint inversion of ground-penetrating radar and thermal-hydrological data from a large-scale underground heater test. Nucl. Technol. 164(2):169–179.

Lambot, S., M. Javaux, F. Hupet, and M. Vanclooster. 2002. A global multilevel coordinate search procedure for estimating the unsaturated soil hydraulic properties. Water Resour. Res. 38(11):1224–1239. doi:1210.1029/2001WR001,224.

Lambot, S., M. Antoine, I. van den Bosch, E.C. Slob, and M. Vanclooster. 2004a. Electromagnetic inversion of GPR signals and subsequent hydrodynamic inversion to estimate effective vadose zone hydraulic properties. Vadose Zone J. 3(4):1072–1081.

Lambot, S., J. Rhebergen, I. van den Bosch, E.C. Slob, and M. Vanclooster. 2004b. Measuring the soil water content profile of a sandy soil with an off-ground monostatic ground penetrating radar. Vadose Zone J. 3(4):1063–1071.

Lambot, S., E.C. Slob, I. van den Bosch, B. Stockbroeckx, and M. Vanclooster. 2004c. Modeling of ground-penetrating radar for accurate characterization of subsurface electric properties. IEEE Trans. Geosci. Remote Sensing 42:2555–2568. doi:10.1109/TGRS.2004.834800

Lambot, S., M. Antoine, M. Vanclooster, and E.C. Slob. 2006a. Effect of soil roughness on the inversion of off-ground monostatic GPR signal for nonin-

vasive quantification of soil properties. Water Resour. Res. 42(3):W03403. .10.1029/2005wr004416.

Lambot, S., E.C. Slob, M. Vanclooster, and H. Vereecken. 2006b. Closed loop GPR data inversion for soil hydraulic and electric property determination. Geophys. Res. Lett. 33:L21405. doi:21,410.21,029/22,006GL027,906.

Lambot, S., L. Weihermüller, J.A. Huisman, H. Vereecken, M. Vanclooster, and E.C. Slob. 2006c. Analysis of air-launched ground-penetrating radar techniques to measure the soil surface water content. Water Resour. Res. 42(11). doi:10.1029/2006WR005097

Lambot, S., E. Slob and H. Vereecken. 2007. Fast evaluation of zero-offset Green's function for layered media with application to ground-penetrating radar. Geophysical Research Letters 34(21): W11403. doi: L2140510.1029/2007GL031459.

Lambot, S., E. Slob, J. Rhebergen, O. Lopera, K.Z. Jadoon, and H. Vereecken. 2009. Remote estimation of the hydraulic properties of a sand using full-waveform integrated hydrogeophysical inversion of time-lapse, off-ground GPR data. Vadose Zone J. 8(3):743–754. doi:10.2136/vzj2008.0058

Lambot, S., E. Slob, J. Minet, K. Z. Jadoon, M. Vanclooster and H. Vereecken. 2010. Full-waveform modelling and inversion of ground-penetrating radar data for non-invasive characterisation of soil hydrogeophysical properties. Proximal soil sensing. Springer, New York.

Lambot, S., F. André, E. Slob, and H. Vereecken. 2012. Effect of antenna medium coupling in the analysis of ground-penetrating radar data. Near Surf. Geophys. doi:10.3997/1873-0604.2012005

Laprise, R. 2008. Regional climate modelling. J. Comput. Phys. 227(7):3641–3666. doi:10.1016/j.jcp.2006.10.024

Ledieu, J., P. De Ridder, P. De Clercq, and S. Dautrebande. 1986. A method of measuring soil moisture by time domain reflectometry. J. Hydrol. 88:319–328. doi:10.1016/0022-1694(86)90097-1

Linde, N., A. Binley, A. Tryggvason, L.B. Pedersen, and A. Revil. 2006. Improved hydrogeophysical characterization using joint inversion of cross-hole electrical resistance and ground-penetrating radar traveltime data. Water Resour. Res. 42:W12404. doi:12,410.11,029/12,006WR005,131.

Looms, M.C., A. Binley, K.H. Jensen, L. Nielsen, and T.M. Hansen. 2008. Identifying unsaturated hydraulic parameters using an integrated data fusion approach on cross-borehole geophysical data. Vadose Zone J. 7(1):238–248. doi:10.2136/vzj2007.0087

Luckner, L., M.T. van Genuchten, and D.R. Nielsen. 1989. A consistent set of parametric models for the 2-phase flow of immiscible fluids in the subsurface. Water Resour. Res. 25(10):2187–2193. doi:10.1029/WR025i010p02187

Lunt, I.A., S.S. Hubbard, and Y. Rubin. 2005. Soil moisture content estimation using ground-penetrating radar reflection data. J. Hydrol. 307(1–4):254–269. doi:10.1016/j.jhydrol.2004.10.014

Malicki, M.A., R. Plagge and C.H. Roth. 1996. Improving the calibration of dielectric TDR soil moisture determination taking into account the solid soil. Eur. J. Soil Sci. 47(3):357–366. doi:10.1111/j.1365-2389.1996.tb01409.x

Mboh, C.M., J.A. Huisman, and H. Vereecken. 2011. Feasibility of sequential and coupled inversion of time domain reflectometry data to infer soil hydraulic parameters under falling head infiltration. Soil Sci. Soc. Am. J. 75(3):775–786. doi:10.2136/sssaj2010.0285

Mboh, C.M., J.A. Huisman, N. Van Gaelen, J. Rings, and H. Vereecken. 2012a. Coupled hydrogeophysical inversion of electrical resistances and inflow measurements for topsoil hydraulic properties under constant head infiltration. Near Surf. Geophys. 10:427–441. doi:10.3997/1873–0604.2012009.

Mboh, C.M., J.A. Huisman, E. Zimmerman, and H. Vereecken. 2012b. Coupled hydrogeophysical inversion of streaming potential signals for unsaturated soil hydraulic properties. Vadose Zone J. 11 doi:10.2136/vzj2011.0115.

Michalski, K.A., and J.R. Mosig. 1997. Multilayered media Green's functions in integral equation formulations. IEEE Trans. Antennas Prop. 45(3):508–519. doi:10.1109/8.558666

Minet, J., P. Bogaert, M. Vanclooster, and S. Lambot. 2012. Validation of ground penetrating radar full-waveform inversion for field scale soil moisture mapping. J. Hydrol. 424-425:112–123. doi:10.1016/j.jhydrol.2011.12.034

Miyamoto, T., T. Annaka, and J. Chikushi. 2003. Soil aggregate structure effects on dielectric permittivity of an andisol measured by time domain reflectometry. Vadose Zone J. 2(1):90–97.

Moysey, S.M.J. 2010. Hydrologic trajectories in transient ground-penetrating radar reflection data. Geophysics 75(4):WA211–WA219.

Mualem, Y. 1976. A new model for predicting the hydraulic conductivity of unsaturated porous media. Water Resour. Res. 12:513–522. doi:10.1029/WR012i003p00513

Nimmo, J.R. 1991. Comment on the treatment of residual water content in "A consistent set of parametric models for the two-phase flow of immiscible fluids in the subsurface" by L. Luckner et al. Water Resour. Res. 27:661–662. doi:10.1029/91WR00165

Priesack, E., and W. Durner. 2006. Closed-form expression for the multimodal unsaturated conductivity function. Vadose Zone J. 5(1):121–124. doi:10.2136/vzj2005.0066

Rhoades, J.D., P.A.C. Raats, and R.J. Prather. 1976. Effects of liquid-phase electrical conductivity, water content, and surface conductivity on bulk soil electrical conductivity. Soil Sci. Soc. Am. J. 40:651–655. doi:10.2136/sssaj1976.03615995004000050017x

Rhoades, J.D., P.J. Shouse, W.J. Alves, N.A. Manteghi, and S.M. Lesch. 1990. Determining soil salinity from soil electrical conductivity using different models and estimates. Soil Sci. Soc. Am. J. 54:46–54. doi:10.2136/sssaj1990.03615995005400010007x

Richards, L.A. 1948. Porous plate apparatus for measuring moisture retention and transmission by soil. Soil Sci. 66(2):105–110. doi:10.1097/00010694-194808000-00003

Roth, C.H., M.A. Malicki, and R. Plagge. 1992. Empirical evaluation of the relationship between soil dielectric constant and volumetric water content as the basis for calibrating soil moisture measurements by TDR. Eur. J. Soil Sci. 43(1):1–13. doi:10.1111/j.1365-2389.1992.tb00115.x

Rucker, D.F. and T.P.A. Ferré. 2004. Parameter estimation for soil hydraulic properties using zero-offset borehole radar: Analytical method. Soil Sci. Soc. Am. J. 68(5):1560–1567. doi:10.2136/sssaj2004.1560

Schaap, M.G., and F.J. Leij. 2000. Improved prediction of unsaturated hydraulic conductivity with the Mualem-van Genuchten model. Soil Sci. Soc. Am. J. 64:843–851. doi:10.2136/sssaj2000.643843x

Schaap, M.G., L. deLange, and T.J. Heimovaara. 1997. TDR calibration of organic forest floor media. Soil Technol. 11(2):205–217. doi:10.1016/S0933-3630(96)00128-6

Scharnagl, B., J.A. Vrugt, H. Vereecken, and M. Herbst. 2011. Inverse modelling of in situ soil water dynamics: Investigating the effect of different prior distributions of the soil hydraulic parameters. Hydrol. Earth Syst. Sci. 15(10):3043–3059. doi:10.5194/hess-15-3043-2011

Simunek, J., M.T. van Genuchten, and M. Sejna. 2008. Development and applications of the HYDRUS and STANMOD software packages and related codes. Vadose Zone J. 7(2):587–600. doi:10.2136/vzj2007.0077

Slob, E., M. Sato, and G. Olhoeft. 2010. Surface and borehole ground-penetrating radar developments. Geophysics 75(5):A103–A120.

Slob, E.C., and J. Fokkema. 2002. Coupling effects of two electric dipoles on an interface. Radio Sci. 37(5):1073–1083. doi:1010.1029/2001RS2529.

Sorooshian, S., Q.Y. Duan, and V.K. Gupta. 1993. Calibration of rainfall-runoff models application of global optimization to the sacramento soil moisture accounting model. Water Resour. Res. 29(4):1185–1194. doi:10.1029/92WR02617

Steelman, C.M., and A.L. Endres. 2011. Comparison of petrophysical relationships for soil moisture estimation using GPR ground waves. Vadose Zone J. 10(1):270–285. doi:10.2136/vzj2010.0040

Stoffregen, H., U. Yaramanci, T. Zenker, and G. Wessolek. 2002. Accuracy of soil water content measurements using ground penetrating radar: Comparison of ground penetrating radar and lysimeter data. J. Hydrol. 267:201–206. doi:10.1016/S0022-1694(02)00150-6

Topp, G., J.L. Davis, and A.P. Annan. 1980. Electromagnetic determination of soil water content: Measurements in coaxial transmission lines. Water Resour. Res. 16:574–582. doi:10.1029/WR016i003p00574

Truss, S., M. Grasmueck, S. Vega, and D.A. Viggiano. 2007. Imaging rainfall drainage within the Miami oolitic limestone using high resolution time-lapse ground-penetrating radar. Water Resour. Res. 43: W03405. doi:10.1029/2005WR004395

van Genuchten, M.T. 1980. A closed-form equation for predicting the hydraulic conductivity of unsaturated soils. Soil Sci. Soc. Am. J. 44:892–898. doi:10.2136/sssaj1980.03615995004400050002x

van Genuchten, M.T., and D.R. Nielsen. 1985. On describing and predicting the hydraulic properties of unsaturated soils. Annales Geophys. 3(5):615–627.

Vereecken, H., J. Maes, J. Feyen, and P. Darius. 1989. Estimating the soil moisture retention characteristic from texture, bulk density, and carbon content. Soil Sci. 148(6):389–403. doi:10.1097/00010694-198912000-00001

Vereecken, H., J.A. Huisman, H. Bogena, J. Vanderborght, J.A. Vrugt, and J.W. Hopmans. 2008. On the value of soil moisture measurements in vadose zone hydrology: A review. Water Resour. Res. 44: W00D06.

Vereecken, H.M. 1995. Estimating the unsaturated hydraulic conductivity from theretical models using simple soil properties. Geoderma 65(1–2):81–92. doi:10.1016/0016-7061(95)92543-X

Vrugt, J.A., H.V. Gupta, W. Bouten, and S. Sorooshian. 2003. A shuffled complex evolution metropolis algorithm for optimization and uncertainty assessment of hydrologic model parameters. Water Resour. Res. 39(8):1201–1217. doi: 1210.1029/2002WR001,642.

Weihermüller, L., J.A. Huisman, S. Lambot, M. Herbst and H. Vereecken. 2007. Mapping the spatial variation of soil water content at the field scale with different ground penetrating radar techniques. J. Hydrol. 340: 205–216. doi:10.1016/j.jhydrol.2007.04.013.

Weynants, M. 2011. Linking soil hydraulic properties to structure indicators experimtents and modelling. Ph.D. thesis. Université catholique de Louvain, Belgium.

Weynants, M., H. Vereecken, and M. Javaux. 2009. Revisiting Vereecken pedotransfer functions: Introducing a closed-form hydraulic model. Vadose Zone J. 8(1):86–95. doi:10.2136/vzj2008.0062